

₁ Study of neutrino-nucleus interaction at around 1 GeV using
₂ a 3D grid-structure neutrino detector, WAGASCI, muon
₃ range detectors and magnetized spectrometer, Baby MIND,
₄ at J-PARC neutrino monitor hall

₅ A. Bonnemaison, R. Cornat, L. Domine, O. Drapier, O. Ferreira, F. Gastaldi,
₆ M. Gonin, J. Imber, M. Licciardi, F. Magniette, T. Mueller, L. Vignoli, and O. Volcy
₇ *Ecole Polytechnique, IN2P3-CNRS, Laboratoire Leprince-Ringuet, Palaiseau,*
₈ *France*

₉ S. Cao and T. Kobayashi

₁₀ *High Energy Accelerator Research Organization (KEK), Tsukuba, Ibaraki, Japan*

₁₁ M. Khabibullin, A. Khotjantsev, A. Kostin, Y. Kudenko, A. Mefodiev, O. Mineev,
₁₂ S. Suvorov, and N. Yershov

₁₃ *Institute for Nuclear Research of the Russian Academy of Sciences, Moscow, Russia*

₁₄ B. Quilain

₁₅ *Kavli Institute for the Physics and Mathematics of the Universe (WPI), The*
₁₆ *University of Tokyo Institutes for Advanced Study, University of Tokyo, Kashiwa,*
₁₇ *Chiba, Japan*

₁₈ T. Hayashino, A. Hiramoto, A.K. Ichikawa, K. Nakamura, T. Nakaya, K Yasutome,
₁₉ and K. Yoshida

₂₀ *Kyoto University, Department of Physics, Kyoto, Japan*

₂₁ Y. Azuma, J. Harada, T. Inoue, K. Kin, N. Kukita, S. Tanaka, Y. Seiya,
₂₂ K. Wakamatsu, and K. Yamamoto

₂₃ *Osaka City University, Department of Physics, Osaka, Japan*

24 A. Blondel, F. Cadoux, Y. Favere, E. Noah, L. Nicola, and S. Parsa

25 *University of Geneva, Section de Physique, DPNC, Geneva, Switzerland*

26 N. Chikuma, F. Hosomi, T. Koga, R. Tamura, and M. Yokoyama

27 *University of Tokyo, Department of Physics, Tokyo, Japan*

28 Y. Hayato

29 *University of Tokyo, Institute for Cosmic Ray Research, Kamioka Observatory,
30 Kamioka, Japan*

31 Y. Asada, K. Matsushita, A. Minamino, K. Okamoto, and D. Yamaguchi

32 *Yokohama National University, Faculty of Engineering, Yokohama, Japan*

33 December 13, 2017

34 **1 Introduction**

35 The understanding of neutrino-nucleus interactions in the 1 GeV energy region is critical
36 for the success of accelerator-based neutrino oscillation experiments such as the T2K exper-
37 iment. Complicated multi-body effects of nuclei render this understanding difficult. The
38 T2K near detectors have been measuring these and significant progress has been achieved.
39 However, the understanding is still limited. One of the big factors preventing from full
40 understanding is the non-monochromatic neutrino beam spectrum. Measurements with
41 different but some overlapping beam spectra would greatly benefit to resolve the contri-
42 bution from different neutrino energies. We, the Wagasci collaboration, proposes to study
43 the neutrino-nucleus interaction at the B2 floor of the neutrino monitor building, where
44 different neutrino spectra can be obtained due to the different off-axis position. Our exper-
45 imental setup contains 3D grid-structure plastic-scintillator detectors filled with water as
46 the neutrino interaction target (Wagasci modules), two side- and one downstream- muon
47 range detectors(MRD's). The 3D grid-structure and side-MRD's allows a measurement of
48 wider-angle scattering than the T2K off-axis near detector (ND280). High water to scintil-
49 lator material ratio enables the measurement of the neutrino interaction on water, which
50 is highly desired for the T2K experiment because it's far detector, Super-Kamiokande,

51 is composed of water. The MRD's consist of plastic scintillators and iron plates. The
52 downstream-MRD, so called the Baby MIND detector, also works as a magnet and pro-
53 vides the charge identification capability as well as magnetic momentum measurement for
54 high energy muons. The charge identification is essentially important to select antineu-
55 trino events in the antineutrino beam because contamination of the neutrino events is as
56 high as 30%. Most of the detectors has been already constructed. The Wagasci modules
57 have been commissioned as the J-PARC T59 experiment and the Baby MIND detector was
58 commissioned at the CERN neutrino platform. Therefore, the collaboration will be ready
59 to proceed to the physics data taking for the T2K beam time in January 2019. We will
60 provide the cross sections of the charged current neutrino and antineutrino interactions on
61 water with slightly higher neutrino energy than T2K ND280 with wide angler acceptance.
62 When combined with ND280 measurements, our measurement would greatly improve the
63 understanding of the neutrino interaction at around 1 GeV and contribute to reduce one
64 of the most significant uncertainty of the T2K experiment.

65 **2 Experimental Setup**

66 Figure. 1 and 2 show a schematic view and a CAD drawing of the entire set of detectors.
67 Central neutrino target detectors consist of two Wagasci modules and T2K INGRID proton
68 module. Inside the Wagasci module, plastic scintillator bars are aligned as a 3D grid-like
69 structure and spaces in the structure are filled with water for a water-in Wagasci module.
70 T2K INGRID proton module is a full active neutrino target detector which is composed
71 only with scintillator bars in its tracking region. The central detectors are surrounded by
72 two side- and one downstream- muon range detectors(MRD's) The MRD's are used to select
73 muon tracks from the charged-current (CC) interactions and to reject short tracks caused by
74 neutral particles that originate mainly from neutrino interactions in material surrounding
75 the central detector, like the walls of the detector hall, neutrons and gammas, or neutral-
76 current (NC) interactions. The muon momentum can be reconstructed from its range
77 inside the detector. The MRD's consist of plastic scintillators and iron plates. In addition,
78 each of the iron plates of the downstream-MRD, so called the Baby MIND detector, is
79 wound by a coil and can be magnetized. It provide the charge selection capability.

80 For all detectors, scintillation light in the scintillator bar is collected and transported
81 to a photodetector with a wavelength shifting fiber (WLS fiber). The light is read out by
82 a photodetector, Multi-Pixel Photon Counter (MPPC), attached to one end of the WLS
83 fiber. The signal from the MPPC is read out by the dedicated electronics developed for the
84 test experiment to enable bunch separation in the beam spill. The readout electronics is
85 triggered using the beam-timing signal from MR to synchronize to the beam. The beam-
86 timing signal is branched from those for T2K, and will not cause any effect on the T2K
87 data taking.

88 T2K adopted the off-axis beam method, in which the neutrino beam is intentionally

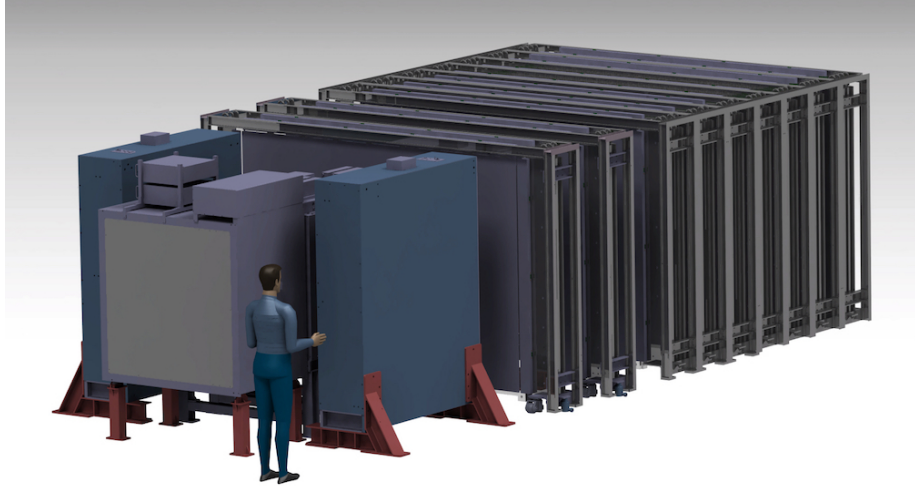


Figure 1: Schematic view of entire sets of detectors.

89 directed 2.5 degrees away from SK producing a narrow band ν_μ beam. The off-axis near
 90 detector, ND280, is installed towards the SK direction in the B1 floor of the near detector
 91 hall of the J-PARC neutrino beam-line. We propose to install our detector in the B2 floor
 92 of the near detector hall, where the off-axis angle is similar but slightly different: 1.5 degree.
 93 The candidate detector position in the B2 floor is shown in Fig. 3. The expected neutrino
 94 energy spectrum at the candidate position is shown in Fig. 4.

95 2.1 Wagasci module

96 The Wagasci module is a neutrino target detector consists of a stainless tank filled with
 97 16 scintillator tracking planes immersed, where each plane is an array of 80 scintillator
 98 bars. The 40 bars, called parallel scintillators, are placed perpendicularly to the beam,
 99 and the other 40 bars, called grid scintillators, are placed in parallel to the beam with grid
 100 structure.

101 The dimension of the each Wagasci module is 100cm \times 100cm in the x and y directions
 102 and 50cm along the beam direction. Thin plastic scintillator bars (thickness \sim 0.3cm)
 103 are used for the Wagasci module to reduce the mass ratio of scintillator bars to water,
 104 because neutrino interactions in the scintillator bars are a background for the cross section
 105 measurements.

106 Inside the Wagasci module, plastic scintillator bars are aligned as a 3D grid-like struc-
 107 ture, shown in Fig. 8.

108 Spaces in the 3D grid-like structure are filled with water for the water-in Wagasci
 109 module. The total water mass serving as neutrino targets in the detector are \sim 0.5 ton.

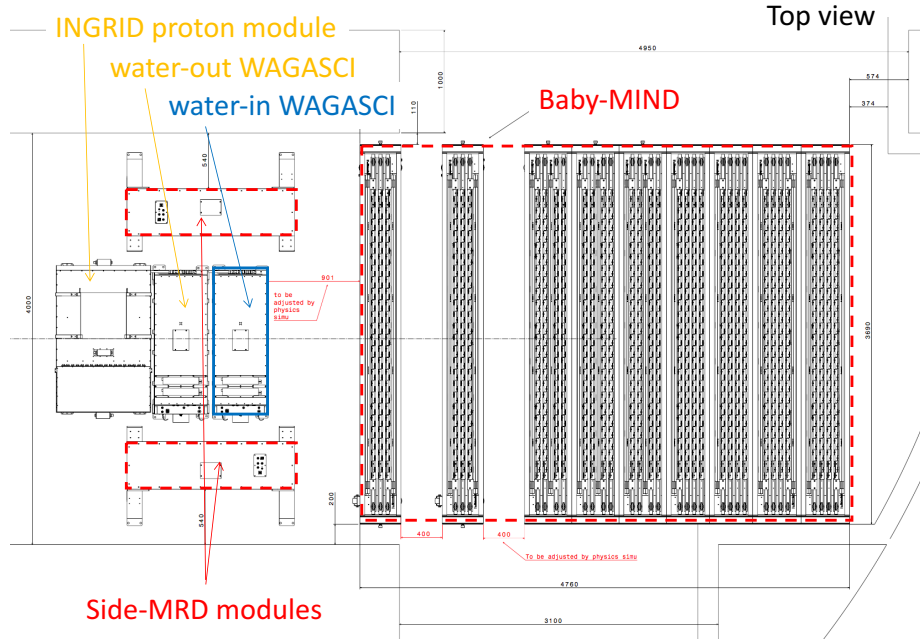


Figure 2: Top view of entire sets of detectors.

When neutrinos interact with hydrogen, oxygen or carbon, in water and scintillators, charged particles are generated. Neutrino interactions are identified by detecting tracks of charged particles through plastic scintillation bars. Thanks to the 3 D grid-like structure of the scintillator bars, the Wagasci module has 4π angular acceptance for charged particles. Furthermore, adopting a 5cm grid spacing, short tracks originated from protons and charged pions can be reconstructed with high efficiency.

Scintillator bars whose dimensions are 2.5cm x 0.3cm x 100cm are used for the Wagasci module. The total number of channels in one Wagasci module is 1280.

2.2 INGRID Proton module

INGRID Proton module is a neutrino detectors of the T2K experiment. It is composed only with scintillator bars in its tracking region. (Add more explanation here.) It was installed at the neutrino beam axis on the SS floor of the T2K near detector hall in 2010, and had been used for neutrino cross section measurements. In August 2017, it was moved to the B2 floor of the same detector hall by J-PARC T59 after getting the approval from T2K to use them. J-PARC T59 is performing neutrino beam measurement using the detector from October 2017, and the measurement will continue until May 2018.

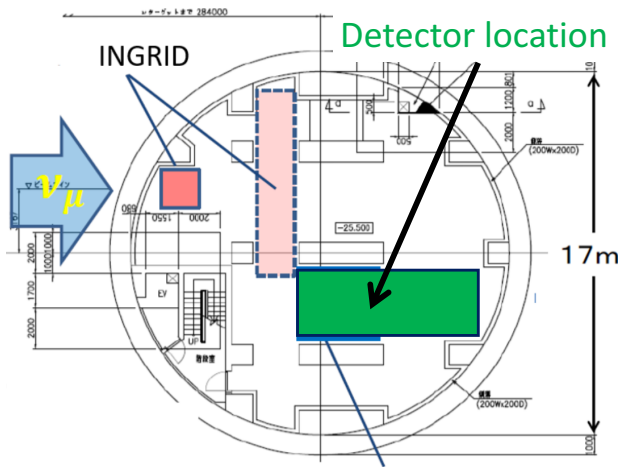


Figure 3: Candidate detector position in the B2 floor of the near detector hall.

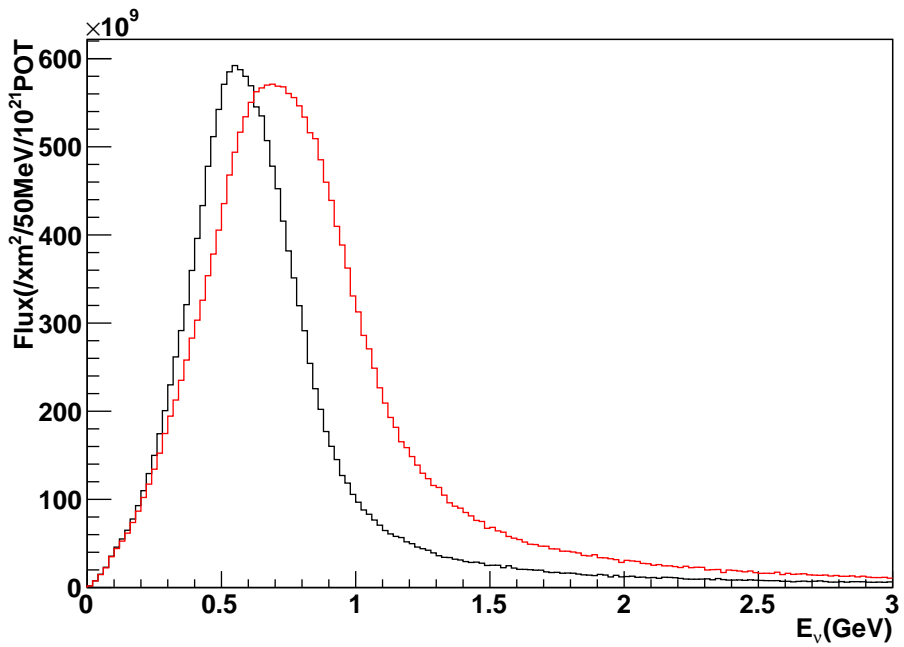


Figure 4: Neutrino energy spectrum at the candidate detector position(red, off-axis 1.5 degree). The spectrum at the ND280 site (black, off-axis 2.5 degree) is also shown.

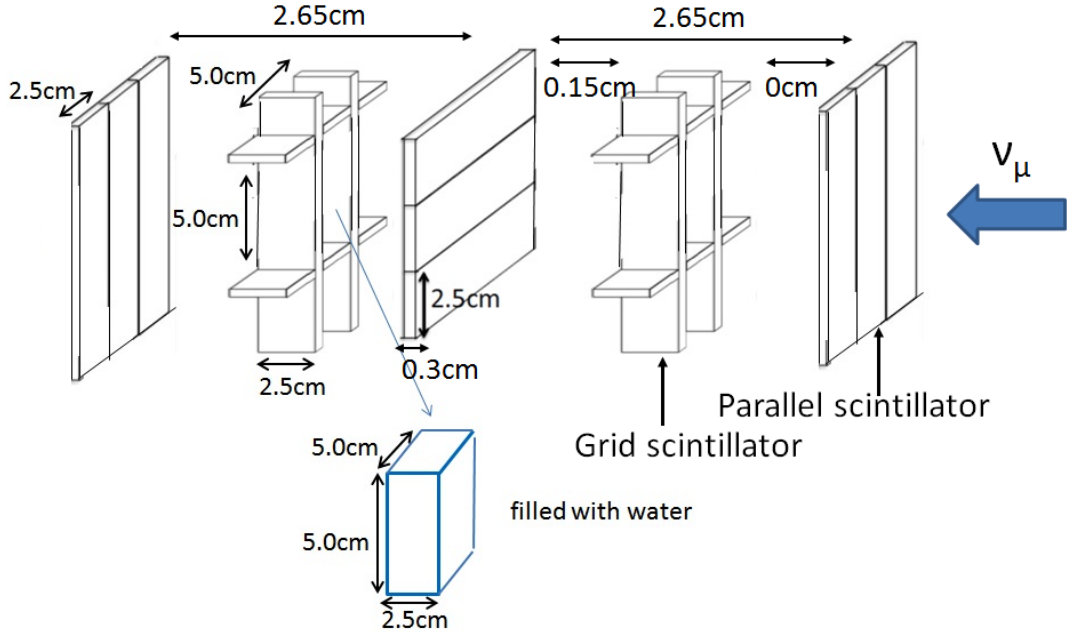


Figure 5: Schematic view of 3D grid-like structure of plastic scintillator bars inside the central detector.

¹²⁶ 2.3 Baby MIND

¹²⁷ The Baby MIND is the downstream Muon Range Detector. It also works as a magnet and
¹²⁸ provides the charge identification capability as well as magnetic momentum measurement
¹²⁹ for high energy muons.

¹³⁰ The Baby MIND collaboration ¹ submitted a proposal to the SPSC at CERN, SPSC-P-
¹³¹ 353. The project was approved by the CERN research board as Neutrino Platform project
¹³² NP05 and constructed. The detector consists of 33 magnet modules, each 3500 mm ×
¹³³ 2000 mm × 50 mm (30 mm steel) with a mass of approximately 2 tonnes. Of these magnet
¹³⁴ modules, 18 are instrumented with plastic scintillator modules.

¹³⁵ 2.3.1 Magnet modules

¹³⁶ The Baby MIND is built from sheets of iron interleaved with scintillator detector modules
¹³⁷ but unlike traditional layouts for magnetized iron neutrino detectors (e.g. MINOS) which
¹³⁸ tend to be monolithic blocks with a unique pitch between consecutive steel segments and
¹³⁹ large conductor coils threaded around the whole magnet volume, the Baby MIND iron seg-

¹Contact person: E. Noah, Spokesperson: A. Blondel, Deputy spokesperson: Y. Kudenko

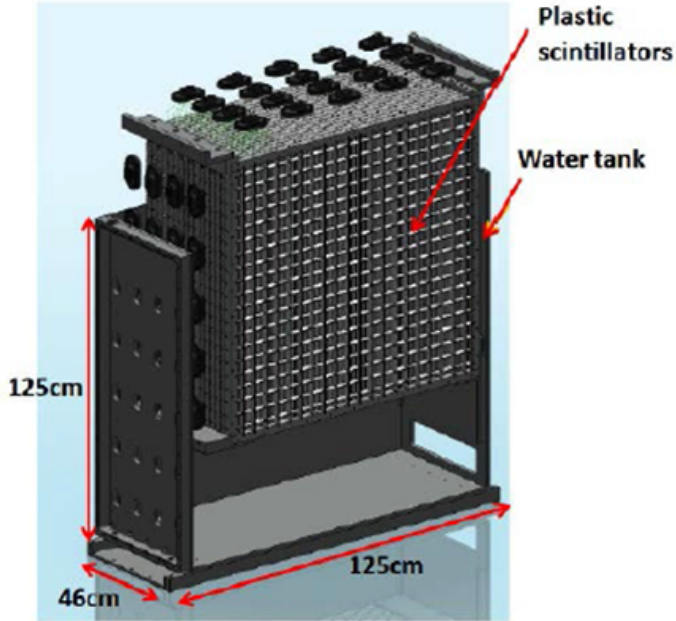


Figure 6: Schematic view of Wagasci module.

¹⁴⁰ ments are all individually magnetized as shown in Fig. 9, allowing for far greater flexibility
¹⁴¹ in the setting of the pitch between segments, and in the allowable geometries that these
¹⁴² detectors can take.

¹⁴³ The key design outcome is a highly optimized magnetic field map. A double-slit config-
¹⁴⁴uration for coil winding was adopted to increase the area over which the magnetic flux
¹⁴⁵lines are homogeneous in B_x across the central tracking region. Simulations show the
¹⁴⁶magnet field map to be very uniform over this central tracking region covering an area of
¹⁴⁷ $2800 \times 2000 \text{ mm}^2$, Fig. 10. The B_x component dominates in this region, with negligible
¹⁴⁸ B_y and B_z . This was confirmed by measuring the field with 9 pick-up coils wound around
¹⁴⁹the first module. Subsequent modules were equipped with one pick-up coil. Test results
¹⁵⁰on the 33 modules show all to achieve the required field of 1.5 T for a current of 140 A,
¹⁵¹with a total power consumption of 11.5 kW. The polarity of the field map shown in Fig. 10
¹⁵²(middle) can be reversed by changing the power supply configuration.

¹⁵³ 2.3.2 Scintillator modules

¹⁵⁴ Each of the 18 scintillator modules is constructed from 2 planes of horizontal counters (95
¹⁵⁵counters in total) and 2 planes of vertical counters (16 counters in total) [?], arranged
¹⁵⁶with an overlap between planes to achieve close to 100% hit efficiency for minimum ioniz-

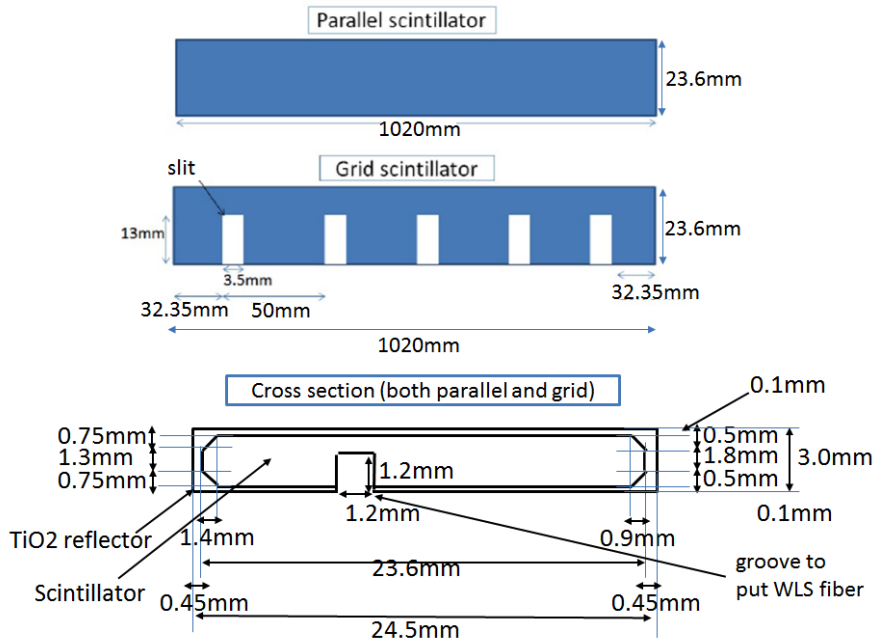


Figure 7: Geometry of scintillators used for Wagasci modules.

157 ing muons. The arrangement of planes within a module is vertical-horizontal-horizontal-
 158 vertical. This arrangement was the result of an assembly approach whereby each plane
 159 was built from 2 half-planes, with each half plane consisting of a horizontal plane and a
 160 vertical plane. The scintillator bars are held in place using structural ladders that align
 161 and maintain the counters, Fig. 11. No glue is used in the process, so counters can be
 162 replaced. Aluminum sheets front and back provide light tightness.

163 The plastic scintillator counters were made from 220 mm-wide slabs, consisting of
 164 extruded polystyrene doped with 1.5% paraterphenyl (PTP) and 0.01% POPOP. They were
 165 cut to size then covered with a 30-100 μm thick diffuse reflector resulting from etching of
 166 the surface with a chemical agent [?, ?]. The horizontal counter size is $2880 \times 31 \times 7.5 \text{ mm}^3$,
 167 with one groove along the length of the bar in which sits a wavelength shifting fiber from
 168 Kuraray. The vertical counter size is $1950 \times 210 \times 7.5 \text{ mm}^3$, with one U-shaped groove
 169 along the bar. On each counter, two custom connectors house silicon photomultipliers,
 170 MPPC type S12571-025C from Hamamatsu, either side of the horizontal counter, and
 171 both connectors at the top for the vertical counter. This geometrical configuration for
 172 vertical counters was chosen for ease of connectivity to the electronics, and maintenance
 173 operations.

174 A total of 1744 horizontal counters and 315 vertical counters (including spares) were

tmp.pdf

Figure 8: tmp.

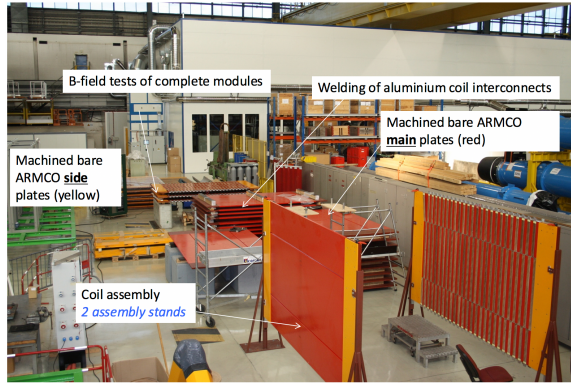


Figure 9: Magnet assembly zone at CERN.

175 produced at the Uniplast company (Vladimir, Russia).

176 2.3.3 Electronics

177 The Baby MIND electronic readout scheme includes several custom-designed boards [?].
178 The revised version is shown in Fig. 12. At the heart of the system is the electronics
179 Front End Board (FEB), developed by the University of Geneva. The readout system
180 includes two ancillary boards, the Backplane, and the Master Clock Board (MCB) whose
181 development has been managed by INRNE (Bulgarian Academy of Sciences) collaborators.

182 The FEBv2 hosts 3 CITIROC chips that can each read in signals from 32 SiPMs [?].
183 Each signal input is processed by a high gain, and a separate low gain, signal path. The
184 outputs from the slow shapers can be sampled using one of two modes: a mode with an
185 externally applied delay, and a peak detector mode. A faster shaper can be switched to

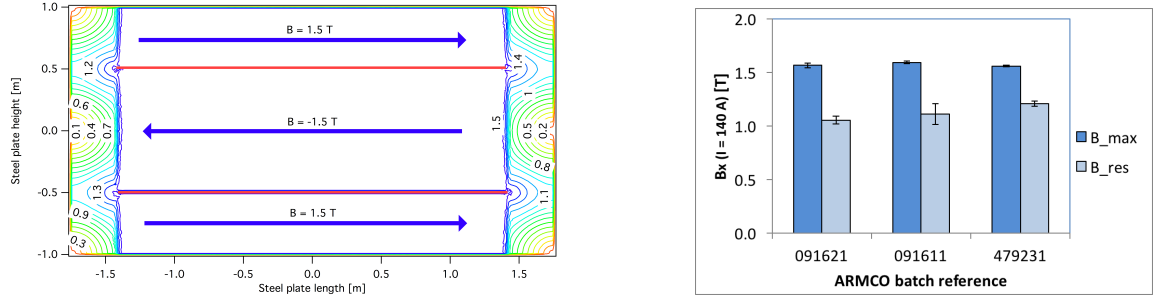


Figure 10: Left) Magnetic field map with a coil along 280 cm of the length of the plate. Right) Measured B field for 33 modules.



Figure 11: Scintillator modules assembly. Left) top of front half-module showing vertical counters, and the spacers-ladders that set the pitch between horizontal counters and hold them in place. Middle) rear half-module showing horizontal counters on their ladders. Right) Assembled rear half-module, the front half-module can be seen in the background.

either HG or LG paths, followed by discriminators with adjustable thresholds providing 32 individual trigger outputs and one OR32 trigger output. An Altera ARIA5 FPGA on the FEBv2 samples these trigger outputs at 400 MHz, recording rising and falling times for the individual triggers and assigning time stamps to these. Time-over-threshold from the difference between falling and rising times gives some measure of signal amplitude, used in addition to charge information and useful if there is more than one hit per bar within the deadtime due to the readout of the multiplexed charge output of $\sim 9 \mu\text{s}$. The ARIA5 also manages the digitization of the sampled CITIROC multiplexed HG and LG outputs via a 12-bit 8-ch ADC.

The internal 400 MHz clock on the FEBv2 can be synchronized to a common 100 MHz clock. The synchronization subsystem combines input signals from the beam line into a digital synchronization signal (SYNC) and produces a common detector clock (CLK) which can eventually be synchronised to an external experiment clock. Both SYNC and CLK signals are distributed to the FEBs. Tests show the FEB-to-FEB CLK(SYNC) delay difference to be 50 ps (70 ps). Signals from the beam line at WAGASCI include two separate timing signals, arriving 100 ms and 30 μs before the neutrino beam at the near

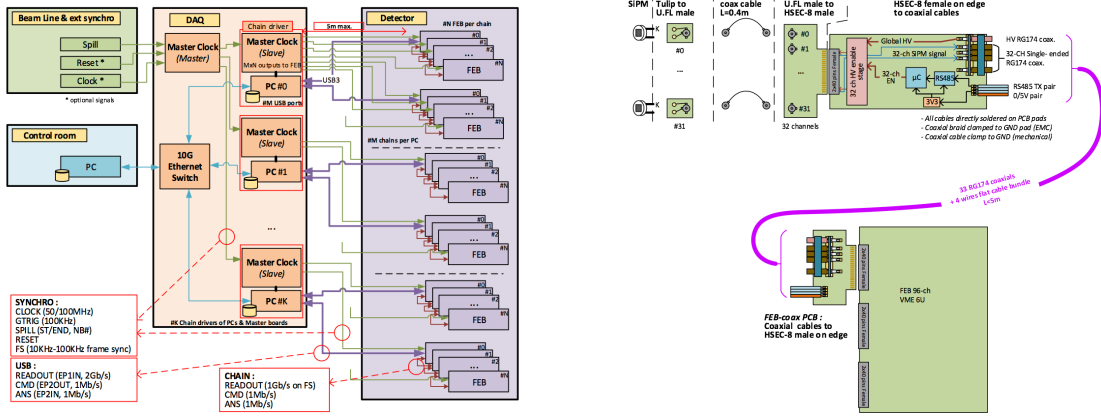


Figure 12: Left) Baby MIND electronics readout scheme. Right) SiPM-to-FEB connectivity.

202 detectors. The spill number is available as a 16-bit signal.

203 The Baby MIND construction was completed in June 2017, and it was then tested in
 204 June and July 2017 at the Proton Synchrotron experimental hall at CERN with a mixed
 205 particle beam comprising mostly muons whose momenta could be selected between 0.5 and
 206 5 GeV/c. An event display from the summer 2017 tests is shown in Fig. 13. All counters
 207 were measured at INR Moscow with a cosmic ray setup using the same type S12571-025C
 208 MPPCs and CAEN DT5742 digitizer [?]. The average light yield (sum from both ends) was
 209 measured to be 37.5 photo-electrons (p.e.) per minimum ionizing particle (MIP) and 65
 210 p.e./MIP for vertical and horizontal counters, respectively. After shipment to CERN, all
 211 counters were tested once more individually with an LED test setup [?]. 0.1% of counters
 212 failed the LED tests and were therefore not used during the assembly of modules.

213 2.4 Side muon range detector

214 Four Side-MRD modules for tracking secondary particles from neutrino interactions will
 215 be constructed by the end of January 2018. Each Side-MRD module is composed of 11
 216 steel plates and 10 layers of total 80 scintillator slabs installed in 13 mm gaps between the
 217 30 mm thick plates. Each steel plate size is $30 \times 1610 \times 1800$ mm 3 . Total module size is
 218 $2236 \times 1630 \times 975$ mm 3 as shown in Fig. 14, weight is ~ 8.5 ton.

219 Scintillator bars were manufactured by Uniplast company in Vladimir, Russia. Polystyrene
 220 based scintillators were extruded with thickness of 7 mm, then cut to the size of $7 \times 200 \times$
 221 1800 mm 3 . Dopant composition is 1.5% PTP and 0.01% POPOP. Scintillator surface was
 222 etched by a chemical agent to form a white diffuse layer with excellent reflective perfor-
 223 mance. Ideal contact between the scintillator and the reflector raises the light yield up to
 224 50% comparing to an uncovered scintillator. Sine like groove was milled along the scin-

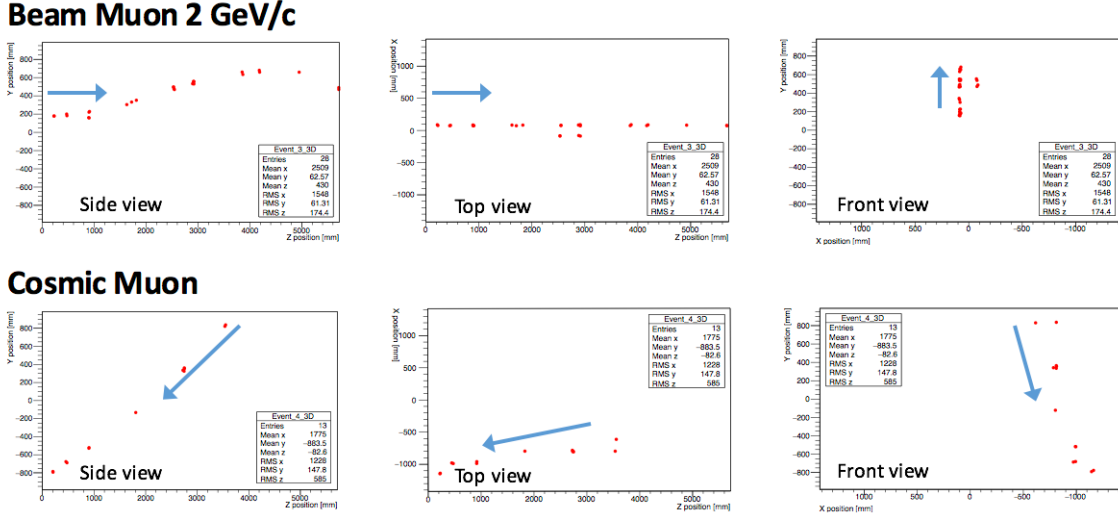


Figure 13: Comparison of a beam muon and cosmic muon in the three different geometrical projections of the detector. The beam impinges on the detector from the left. The arrows indicate the direction of travel of these muons. The direction of the cosmic muon is inferred from timing information.

tillator to provide uniform light collection over the whole scintillator surface. WLS Y11 Kuraray fiber of 1 mm diameter is glued with an optical cement EJ-500 in the S-shape groove as shown in Fig. 15. Bending radius is fixed to 30 mm that was specified to be safe for Kuraray S-type fibers. Both ends of the fiber are glued into optical connectors (Fig. 16) which mounted within a scintillator body.

The plastic molded connectors provide an interface to SiPMs, Hamamatsu MPPC S13081-050CS(X1) used for the WAGASCI detector. Optical coupler of this type (so-called Baby-mind type of optical connector) consists of two parts (see Fig. 16): a container for the MPPC and a ferrule with the fiber. The ferrule is glued in the scintillator, and its end with glued in WLS fiber was polished. Both parts of the optical coupler are latched by a snap-like mechanism: a locking groove inside the container and matching ring protuberance on the ferrule. To ensure the optical contact a foam spring made of sponge rubber presses the MPPC to the fiber end (Fig. 17).

Scintillators for the Side-MRD modules had been assembled at INR in Russia, and shipped to Japan in July 2017. The light yield for each scintillator was measured with cosmic rays at INR and at YNU in Japan after delivery. Parameters measured at the center of the counter were : the light yields LY_1 and LY_2 at both ends, the light yield asymmetry between the ends calculated as $100\% \times \frac{LY_1 - LY_2}{LY_1 + LY_2}$. After tests at INR we selected 324 counters from measured 332 ones with the mean light yield of 45 p.e./MIP ($LY_1 + LY_2$) and the asymmetry value less than 10 %. The measurements at YNU yielded the average

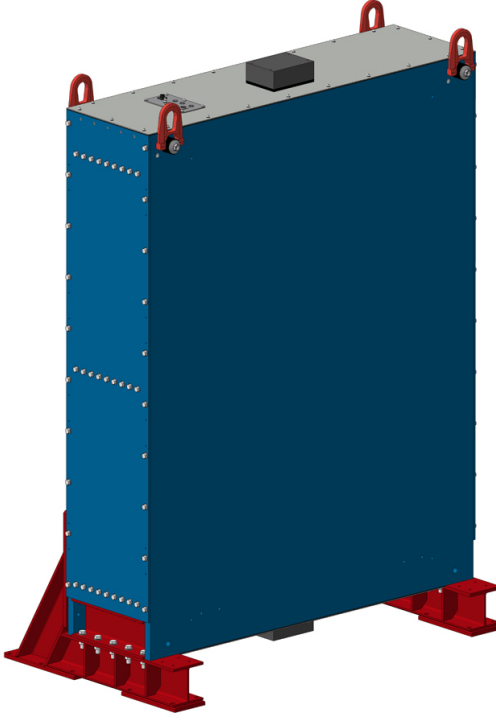


Figure 14: Support structure of the Side-MRD module.

total light yield of about 40 p.e./MIP which varies in range from 32 to 50 p.e/MIP (Fig. 18 (left)). Only two counters showed relatively high asymmetry close to 25 % as shown in Fig. 18 (right). Using the results of the quality assurance test we selected 320 scintillator counters for the Side-MRD modules.

We also measured the time resolution for a combination of four counters piled each on another one. Time resolution for a single counter is determined as rms of $(T_{left} - T_{right})/2$ distribution. The difference of times was chosen to remove the correlated time fluctuation caused by a start trigger signal. The average result for four counters is $\sigma_T = 1.04$ ns (Upper left plot in Fig. 19). For a set of n counters the time resolution is calculated as $\frac{(T_L - T_R)_1 + (T_L - T_R)_2 + \dots + (T_L - T_R)_n}{2 \times n}$. The result of combination of 2, 3, 4 counters is 0.79 ns, 0.66 ns and 0.58 ns, correspondently (Fig. 19).

Construction of Side-MRD modules will be done from November 2017 to January 2018 at Yokohama National University, then they will be transported to J-PARC and will be installed at B2 floor of the T2K near detector hall before T2K beam in March 2018.

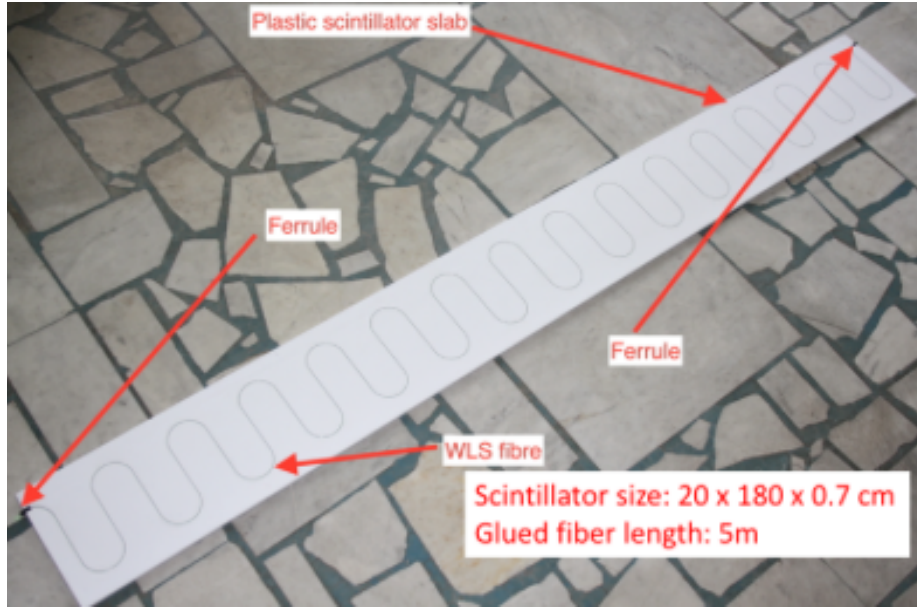


Figure 15: Scintillator bar of the Side-MRD modules.

259 3 Physics goals

260 We will measure the differential cross section for the charged current interaction on H₂O
 261 and Hydrocarbon(CH)). The water-scintillator mass ratio of the Wagasci module is as
 262 high as 5:1 and the high purity measurement of the cross section on H₂O is possible. One
 263 experimental option is to remove water from one of the two Wagasci modules. The water-
 264 out WAGASCI module will allow to measure pure-CH target interactions with very low
 265 momentum-threshold for protons. It will also benefit to subtract the background from
 266 interaction with scintillator in the water target measurement. Another option is to add
 267 the T2K proton module which is fully made of plastic scintillators. It will allow the high
 268 statistics comparison of cross section between H₂O and CH and also comparison with
 269 the ND280 measurement. The actual configuration will be optimized with detailed MC
 270 simulation by 2018 Summer.

271 Our setup allows the measurements of inclusive and also exclusive channels such as 1- μ ,
 272 1- $\mu 1p$, 1- $\mu 1\pi \pm np$ samples, former two of which are mainly caused by the quasi-elastic and
 273 2p2h interaction and the latter is mainly caused by resonant or coherent pion production
 274 and deep elastic scattering. In general, an accelerator produced neutrino beam spectrum
 275 is wide and the energy reconstruction somehow rely on the neutrino interaction model.

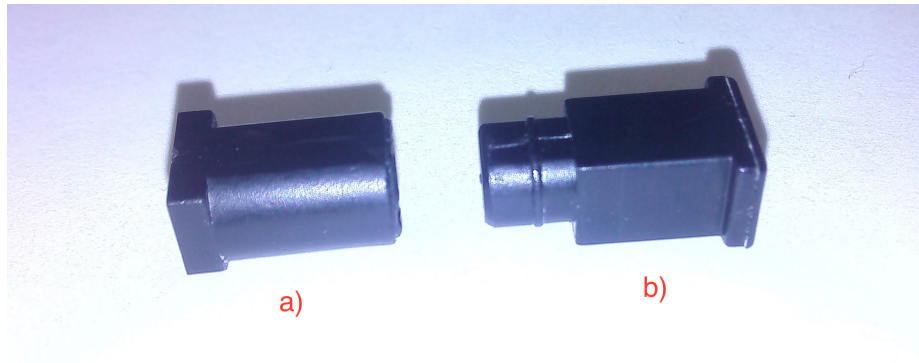


Figure 16: Optical connector for the Side-MRD scintillator. a) MPPC cover. b) Ferrule.

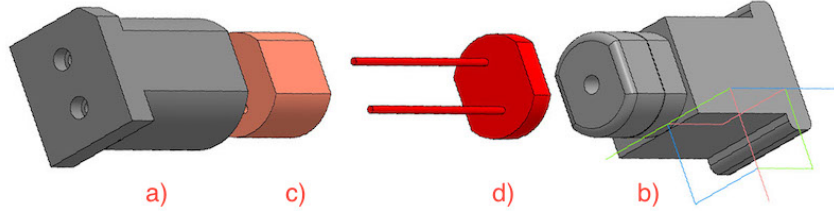


Figure 17: Scheme of the MPPC placement in optical connector. a) MPPC cover. b) Ferrule. c) Spring (sponge rubber). d) MPPC.

276 Therefore, recent neutrino cross section measurement results including those from T2K
 277 are given as a flux-integrated cross section rather than cross sections as a function of
 278 the neutrino energy to avoid the model dependency. We can provide the flux-averaged
 279 cross section. In addition, by combining our measurements with those at ND280, model-
 280 independent extraction of the cross section for narrow energy region becomes possible.
 281 This method was demonstrated in [?] and also proposed by P** (NUPRISM).

282 3.1 Expected number of events

283 Expected number of neutrino events after the event selections is evaluated with Monte
 284 Carlo simulations as we will discuss in Section 5. In the neutrino-mode, 4.2×10^3 , 1.1×10^3
 285 and $\sim 3.8 \times 10^3$ CC neutrino events are expected in the water-in WAGASCI module, the
 286 water-out WAGASCI module and the INGRID proton module after the selections with
 287 0.5×10^{21} POT, and its purities are 78.0 %, 97.5 % and $\sim 98\%$. In the antineutrino-mode,
 288 1.7×10^3 , 0.4×10^3 and $\sim 1.5 \times 10^3$ CC antineutrino events are expected in the water-in

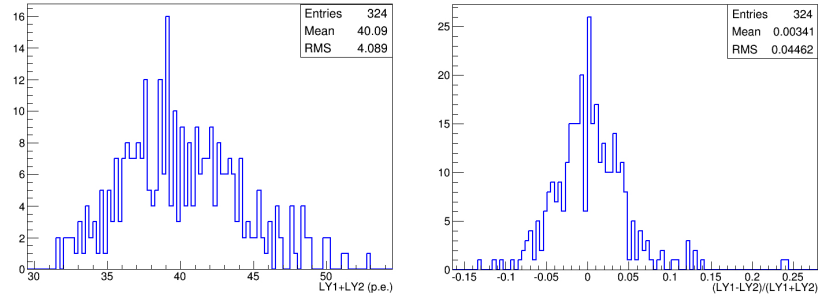


Figure 18: Total light yield distribution (left) and light yield assymetry (right) measured at YNU.

289 WAGASCI module, the water-out WAGASCI module and the INGRID proton module
 290 after the selections with 0.5×10^{21} POT, and its purities are 59.5 %, 74.4 % and $\sim 74\%$.

291 Statical errors of flux integrated CC-inclusive neutrino cross section measurements on
 292 H₂O (full acceptance) and CH targets (forward acceptance) will be $\sim 1.5\%$ and $\sim 1.6\%$
 293 with 0.5×10^{21} POT in the neutrino-mode. Statical errors of flux integrated CC-inclusive
 294 antineutrino cross section measurements on H₂O (full acceptance) and CH targets (forward
 295 acceptance) will be $\sim 2.4\%$ and $\sim 2.5\%$ with 0.5×10^{21} POT in the neutrino-mode.

296 Statical errors of flux integrated H₂O to CH CC-inclusive neutrino cross section ratio
 297 measurement will be $\sim 3.1\%$ (full acceptance) and $\sim 2.3\%$ (forward acceptance) with
 298 0.5×10^{21} POT in the neutrino-mode. Statical errors of flux integrated H₂O to CH CC-
 299 inclusive antineutrino cross section ratio measurement will be $\sim 5\%$ (full acceptance) and
 300 $\sim 3.7\%$ (forward acceptance) with 0.5×10^{21} POT in the neutrino-mode.

301 3.2 Pseudo-monochromatic beam by using different off-axis fluxes

302 The off-axis method gives narrower neutrino spectrum, and the peak energy is lower for
 303 larger off-axis angle. There still remains high energy tail mainly due to neutrinos from
 304 Kaon decay. The off-axis angle of the Wagasci location is 1.5 degree and different from the
 305 ND280 2.5 degree. Top two plots of Fig. 20 show the energy spectra of fluxes and neutrino
 306 interaction events at these two different location. The high energy tail of ND280 flux can
 307 be somehow subtraction by using the Wagasci measurement. The low energy part of the
 308 Wagasci flux can be also subtracted by using the ND280 measurement. Bottom two plots
 309 of Fig. 20 demonstrate this method. We can effectively get two fluxes, from 0.2 GeV to
 310 0.9 GeV and 0.6 GeV and 2 GeV and measure flux-integrated cross section for these two
 311 fluxes.

312 Statical errors of flux integrated CC-inclusive neutrino cross section measurements
 313 on H₂O (forward acceptance) and CH targets (forward acceptance) with the pseudo-

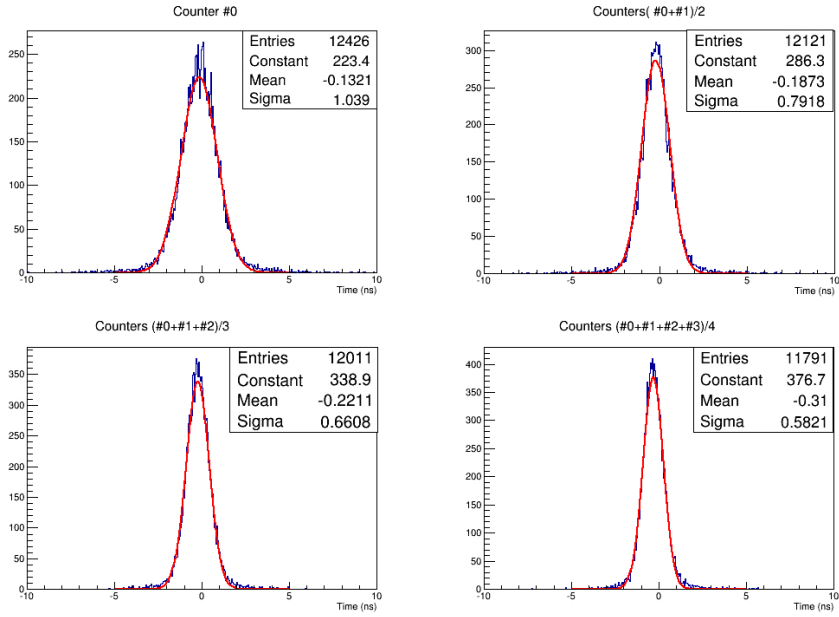


Figure 19: Time resolution for one (upper left) and a set of 2,3,4 Side-MRD counters.

314 monochromatic beam will be $\sim 2\%$ and $\sim 1.9\%$ with 0.5×10^{21} POT in the neutrino-
 315 mode. Statical errors of flux integrated CC-inclusive antineutrino cross section measure-
 316 ments on H₂O (full acceptance) and CH targets (forward acceptance) with the pseudo-
 317 monochromatic beam will be $\sim 3\%$ and $\sim 2.8\%$ with 0.5×10^{21} POT in the neutrino-
 318 mode.

319 3.3 Subjects Wagasci can contribute

320 In T2K experiment, neutrinos interact with bound nucleons in relatively heavy nuclei
 321 (Carbon and Oxygen), so the cross-section is largely affected by nuclear effects. The nuclear
 322 effects are categorized as nucleons' momentum distribution in nucleus, interactions with
 323 correlated pairs of nucleons in nucleus (two particles-two holes, 2p2h), collective nuclear
 324 effects calculated with Random Phase Approximation (RPA) and final state interactions
 325 (FSI) of secondary particles in the nuclei after the initial neutrino interactions.

326 The 2p2h interactions mainly happen through Δ resonance interactions following a
 327 pion-less decay and interactions with a correlated nucleon pair. The 2p2h interactions are
 328 observed in electron scattering experiments (add ref. here) where the 2p2h events observed
 329 in the gap between Quasi-Elastic region and Pion-production region as shown in Fig. ???.
 330 Neutrino experiments also attempt to measure the 2p2h interactions, but separation of the

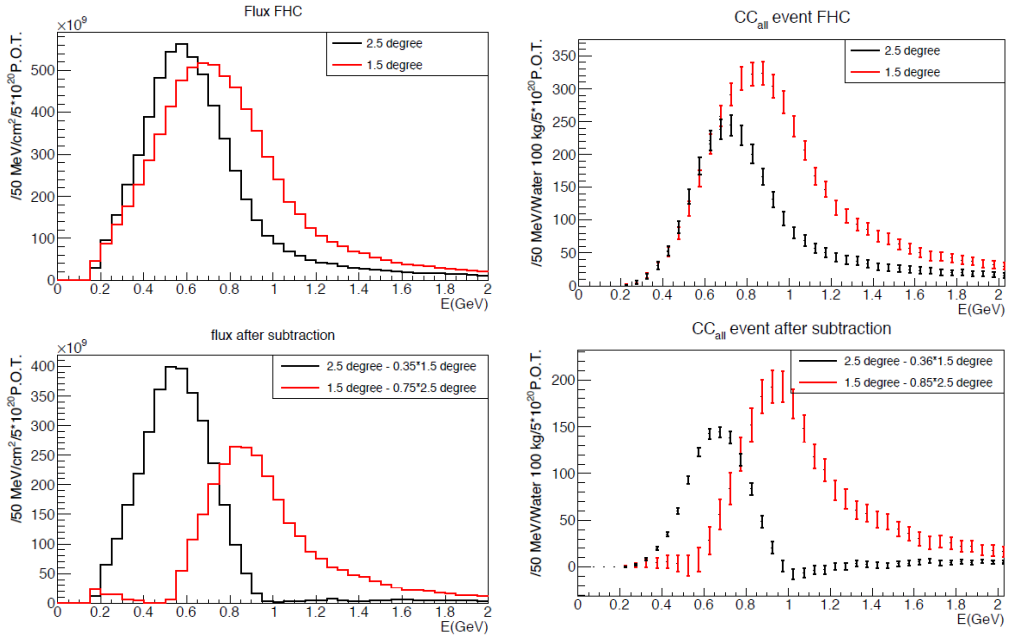


Figure 20: Energy spectra obtained by using different off-axis angle fluxes. Top two plots show the fluxes(left) and spectra of interaction events (right) for ND280 (off-axis 2.5 degree) and Wagasci (off-axis 1.5 degree). Bottom two plots show the fluxes (left) and spectra of interaction events (right) obtained by subtraction of fluxes at ND280 and Wagasci. The error bar is for the statistical error and those in the bottom right plot is obtained assuming the statistical error for ND280 measurement is much smaller than that of Wagasci experiment.

331 QE peak and the 2p2h peak is more difficult because transferred momentum (p) and energy
 332 (w) are largely affected by neutrino energies which cannot be determined event-by-event in
 333 the wide energy spectrum of the accelerator neutrino beam. Our model-independent narrow
 334 neutrino spectra extracted from combined analyses of our data and ND280 data are ideal
 335 for searching the 2p2h interaction because clearer separation of the QE peak and the 2p2h
 336 peak is expected. Another way to observe the 2p2h interaction is direct measurement of
 337 proton tracks in CC π sample with low detection threshold and full acceptance. Fig. ??
 338 shows proton multiplicities in CCQE events and 2p2h events, and Fig. ?? shows opening
 339 angles among two proton tracks in the same samples. The water-out WAGASCI can provide
 340 good sample for the 2p2h interaction search because its low density medium enables the
 341 detection of low momentum protons in addition to the full acceptance.

342 The corrections from collective nuclear effects calculated by RPA as a function of Q^2 are
 343 shown in Fig. ???. The Q^2 dependence of the correction can be tested by measuring angular

344 distribution of muons in CC1- μ and CC1- $\mu 1p$ events. The uncertainties of the corrections
345 in low (high) Q^2 regions can be constrained by observing the events with a forward-going
346 (high-angle) muon, so it is essential to measure muon tracks with full acceptance.

347 T2K experiment is starting to use ν_e CC1 π events for its CP violation search to increase
348 the statistics. One of the biggest uncertainty of the CC1 π sample comes from the final
349 state interactions of pions in the nuclei after the initial neutrino interactions because they
350 change the multiplicity, charge and kinematics of the pions. The multi-pion production
351 events can be migrated into the CC1 π sample due to the FSIs, and they become important
352 backgrounds. We can constrain the uncertainties from the pion FSIs by measuring pion
353 rescattering in the detector and pion multiplicity in ν_μ CCn π sample with low detection
354 threshold and full acceptance for pion tracks. The water-out WAGASCI can provide good
355 sample for the pion FSI studies because its low density medium enables the detection of
356 low momentum pions in addition to the full acceptance.

357 4 Status of J-PARC T59 experiment

358 We had submitted a proposal of a test experiment to J-PARC in April 2014 to test a new
359 detector with a water target, WAGASCI, at the neutrino monitor hall, and the proposal
360 was approved as J-PARC T59. The project contains the side and downstream muon range
361 detectors as well.

362 The first WAGASCI module has been constructed in 2016 and installed at the on-
363 axis position in front of the T2K INGRID detector for the commissioning and the first
364 cross section measurement as a part of the T2K experiment. The INGRID electronics
365 boards are used to read the signal. The light yield measured with muons produced by
366 the interaction of neutrinos in the hall wall, shown in Fig. 21, is sufficiently high to get
367 good hit efficiency. A track search algorithm based on the cellular automaton has been
368 developed using the software tools by the T2K INGRID. Examples of observed events are
369 shown in Fig. 22. The tracking efficiency in 2-dimensional projected plane was evaluated
370 by comparing the reconstructed track in the WAGASCI module and the INGRID module
371 and shown in Fig. 23. Note that that the tracking efficiency for high angle (> 70 deg) is not
372 evaluated because of the acceptance of the INGRID module, not because of the limitation
373 of the WAGASCI module.

374 In 2017 Autumn, the construction of the second WAGASCI module and the dedicated
375 electronics board were completed. The module and the electronics were install to the B2
376 floor together with the T2K proton module and the INGRID module as shown in Fig. 24.
377 The proton module is to be used as the entering muon veto and also for the comparison
378 of interaction between CH and Water. The INGRID module is for the temporary muon
379 detector with limited acceptance for this period. The detector was commissioned and is
380 in operation to take data with the antineutrino beam during the T2K beam time from
381 October.

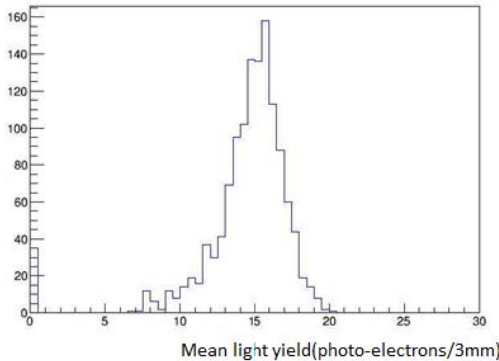


Figure 21: Light yield for muons produced by the interaction of neutrinos in the hall wall. Average light yields for each channel are plotted.

382 The production of the components of the side muon range detectors has been completed
 383 and now the detectors are being assembled at the Yokohama National University. These
 384 detectors will be installed sometime from January to June, 2018 when T2K is not running.

385 The Baby MIND detector was transported from CERN to Japan in December, 2017.
 386 It will be installed and commissioned in Jan.-Feb. 2018 and T59 will take the neutrino-
 387 induced muon data in April and May.

388 5 MC studies

389 5.1 Detector simulation

390 Expected number of neutrino events in the water-in Wagasci detector is evaluated with
 391 Monte Carlo simulations. Neutrino beam flux at the detector location is simulated by
 392 T2K neutrino flux generator, JNUBEAM, neutrino interactions with target materials are
 393 simulated by a neutrino interaction simulator, NEUT, detector responses are simulated
 394 using GEANT4-based simulation. The neutrino flux at the detector location, 1.5 degrees
 395 away from the J-PARC neutrino beam axis, is shown in Figure 4, and its mean neutrino
 396 energy is around 0.68 GeV.

397 5.1.1 Detector geometry

398 The detector geometry in the GEANT4-based simulation is slightly different from the
 399 actual detector as shown in Fig. 26. The active neutrino target region consists of four
 400 Wagasci modules, and each Wagasci detector has the dimension with 100 cm × 100 cm in
 401 the x and y directions and 50 cm along the beam direction. An event display of a MC event

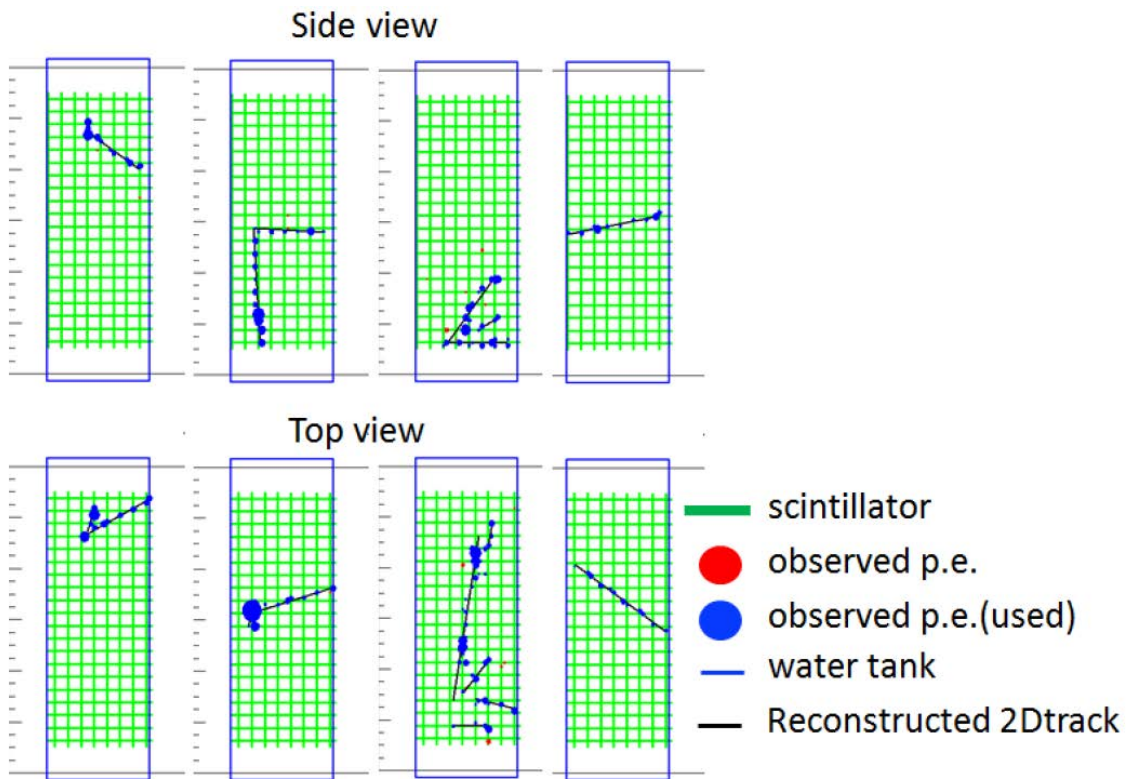


Figure 22: Example event displays of the WAGASCI module at on-axis. The reconstructed tracks are overlaid.

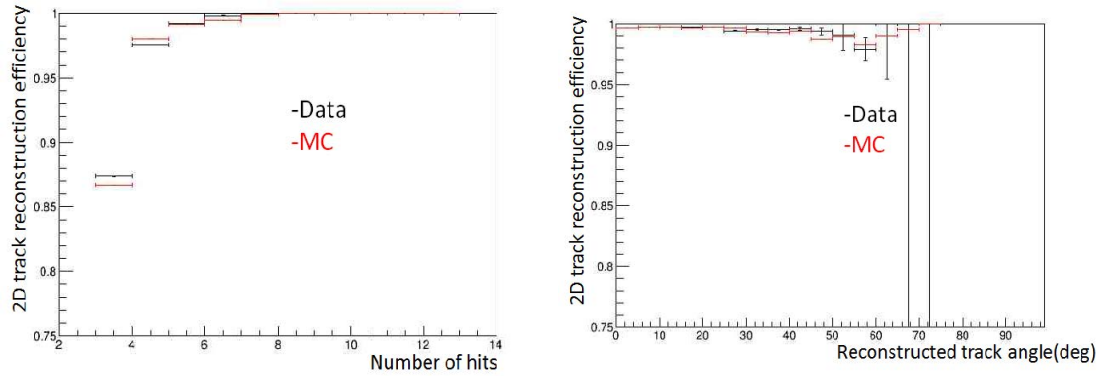


Figure 23: 2D track reconstruction efficiency as a function of number of hits (left) and track angle (right). Here the track angle is the one reconstructed by the INGRID module.

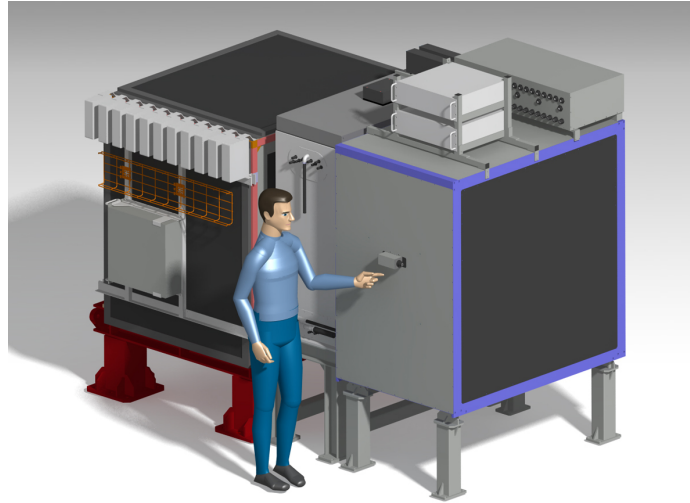


Figure 24: J-PARC T59 detector configuration in October 2017.

402 in the Wagasci detectors is shown in Figure ???. Two Side-MRD modules is installed at
 403 both sides of the Wagasci modules, and each Side-MRD module consists of ten iron plates
 404 whose dimension is 3 cm (thickness) \times 200 cm (height) \times 320 cm (width). The distance
 405 between the Side-MRD modules and Wagasci modules is 80 cm. The downstream-MRD
 406 equivalent to the Baby-MIND is installed at the downstream of the Wagasci modules. The
 407 downstream-MRD consists of thirty iron plates whose dimension is 3 cm (thickness) \times 200
 408 cm (height) \times 400 cm (width). The distance between the downstream-MRD modules and
 409 Wagasci modules is 80 cm.

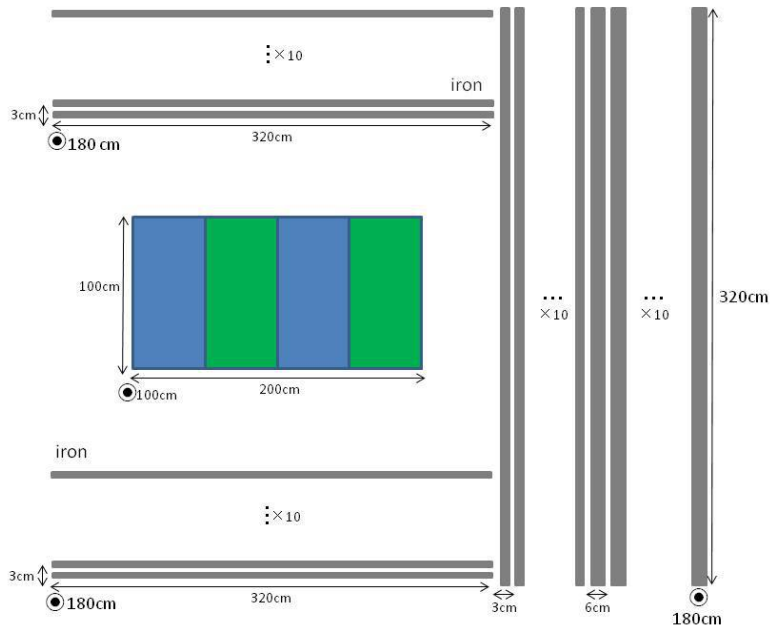


Figure 25: Geometry of the detectors in the Monte Carlo simulation.

410 5.1.2 Response of detector components

411 The energy deposit inside the scintillator is converted into the number of photons. The
 412 effects of collection and attenuation of the light in the scintillator and the WLS fiber are
 413 simulated, and the MPPC response is also taken into account. The light yield is smeared
 414 according to statistical fluctuations and electrical noise.

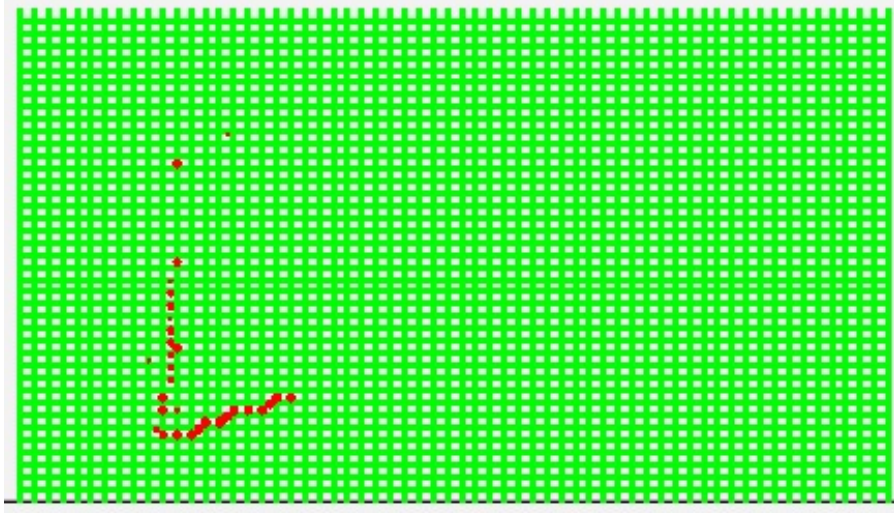


Figure 26: An event display of MC event in Wagasci detectors. Green lines are scintillators and red circles are the hit channels.

415 **5.2 Track reconstruction**

416 To select neutrino interaction from the hit patterns, a track reconstruction algorithm is
417 developed. The flow of the track reconstruction is as follows.

- 418 1. Two-dimensional track reconstruction in each sub-detectors
- 419 2. Track matching among the sub-detectors
- 420 3. Three -dimensional track reconstruction

421 Add explanation about two-dim reco, track matching and three-dim reco here.

422 **5.3 Event selection**

423 First, the events with the track which starts in 5 cm from the wall of the Wagasci module
424 are rejected to remove the background from the outside.

425 Second, to reject backgrounds from NC and neutral particles, the longest tracks are
426 required to penetrate more than one (five) iron plates in Side-MRD modules (Baby-MIND).
427 Then, in order to measure muon momentum, the longest tracks are required to stop in
428 MRDs (Side-MRD modules and Baby-MIND) or penetrate all iron plates.

429 Table 1 and 2 show numbers of the selected events in one water-in Wagasci module
430 after each event selection in neutrino-mode and antineutrino-mode respectively. As for
431 the neutrino-mode, 8478 CC events are expected with 1×10^{21} POT, and the purity is

432 78.0 %. The main background for the neutrino-mode is the neutrino interactions in the
 433 scintillators inside the Wagasci detector. As for the antineutrino-mode, 3331 CC events
 434 are expected with 1×10^{21} POT, and the purity is 59.5 %. The main background for the
 435 antineutrino-mode is the wrong sign contamination from ν_μ events and the antineutrino
 436 interactions in the scintillators inside the Wagasci detector.

Table 1: Expected number of the neutrino-candidate events in one water-in Wagasci module with 1×10^{21} POT in neutrino-mode.

Cut	CC	NC	Scinti Bkg.	Total
Reconstructed	18093.2	699.7	4698.3	23491.2
FV	15150.8	588.4	3934.8	19673.9
Pene. iron	11264.3	237.3	2875.4	14377.0
Stop/Penetrate MRDs	8478.2	214.0	2173.1	10865.2
after all cuts	78.0 %	2.0 %	20.0 %	100 %

Table 2: Expected number of the antineutrino-candidate events in one water-in Wagasci module with 1×10^{21} POT in antineutrino-mode.

Cut	CC	NC	Scinti Bkg.	Wrong sign bkg	Total
Reconstructed	6499.7	107.3	2234.4	2330.8	11172.1
FV	5457.9	89.3	1873.5	1946.6	9367.1
Pene. iron	4172.3	30.8	1440.9	1560.6	7204.6
Stop/Penetrate MRDs	3331.5	28.5	1120.3	1121.2	5601.5
after all cuts	59.5 %	0.5 %	20.0 %	20.0 %	100 %

437 Table 3 and 4 show numbers of the charged-current events in the water-in Wagasci
 438 module after all event selection with a classification based on interactions at a vertex with
 439 1×10^{21} POT in neutrino-mode and antineutrino-mode respectively.

Table 3: Expected number of the charged-current events in the water-in Wagasci module after the event selections with 1×10^{21} POT in neutrino-mode with a classification based on interactions at a vertex.

CCQE	MEC	CCRes	CCDIS	Total
3716.3	747.0	2081.3	1132.3	7676.9
48.4 %	9.7 %	27.1 %	14.7 %	100 %

Table 4: Expected number of the charged-current events in the water-in Wagasci module after the event selections with 1×10^{21} POT in antineutrino-mode with a classification based on interactions at a vertex.

CCQE	MEC	CCRes	CDDIS	Total
2522.0	362.8	765.8	765.8	4416.4
hline 57.1 %	8.2 %	17.3 %	17.3 %	100 %

440 Table 5 and 6 show numbers of the charged-current events in one water-in Wagasci
 441 module after all event selection with a classification based on particles after final state
 442 interactions with 1×10^{21} POT in neutrino-mode and antineutrino-mode respectively.

Table 5: Expected number of the charged-current events in one water-in Wagasci module after the event selections with 1×10^{21} POT in neutrino-mode with a classification based on particles after final state interactions.

CC0 π	CC1 π	CC2 π	CCn π	Total
5423.1	1684.3	242.9	701.1	8051.4
67.4 %	20.9 %	3.0 %	8.7 %	100 %

Table 6: Expected number of the charged-current events in one water-in Wagasci module after the event selections with 1×10^{21} POT in antineutrino-mode with a classification based on particles after final state interactions.

CC0 π	CC1 π	CC2 π	CCn π	Total
2529.3	520.0	37.9	96.0	3183.2
79.5 %	16.3 %	1.2 %	3.0 %	100 %

443 Figure 27 and 28 show the reconstructed angles of the longest tracks in the selected
 444 events in the neutrino-mode and the anti-neutrino mode respectively. Figure 29, 30 31
 445 and 32 show the iron plane numbers in Side-MRD and Baby-MIND corresponding to the
 446 end points of the longest tracks in the selected events in the neutrino-mode and the anti-
 447 neutrino mode.

448 5.4 Cross section measurements on water

449 In the water target events, the background from interaction with scintillators has to be
 450 subtracted by using the measurement of the hydrocarbon target.

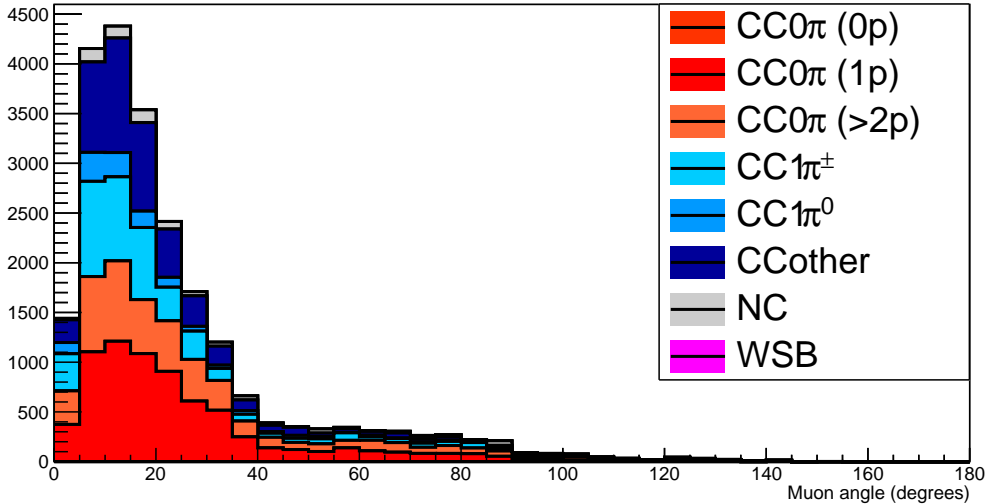


Figure 27: The reconstructed angles of the longest tracks in the selected events in the neutrino-mode.

451 5.4.1 Charged current cross section measurement

452 6 Standalone WAGASCI-module performances

453 In the previous sections, the WAGASCI detector was studied using the Muon Range Detectors. In this section, the standalone abilities of WAGASCI module are presented. Using
 454 the WAGASCI configuration presented in Section 5, we have evaluated that only 7% of
 455 the muons will be stopped in one of the WAGASCI modules. THowerver, this proportion
 456 increases to 53% for pions and 73% for protons produced by neutrino interactions at 1.5°
 457 off-axis. Figure 33 shows the momentum distribution of these daughter particles as well as
 458 for the sub-sample stopped in one of the WAGASCI modules. Therefore, the study of the
 459 standalone abilities of the WAGASCI module in this section are dominantly motivated by:
 460

- 461 • the accurate measurement of the neutrino interaction final states. Though most of the
 462 muons will be reconstructed and identified in the MRDs, the hadronic particles will
 463 predominantly stops in one WAGASCI module. One has therefore to rely exclusively
 464 on the WAGASCI module information alone to reconstruct, identify and measure the
 465 momentum of pions or protons.
- 466 • the coverage of the MRDs is not 4π . Using the WAGASCI module information can

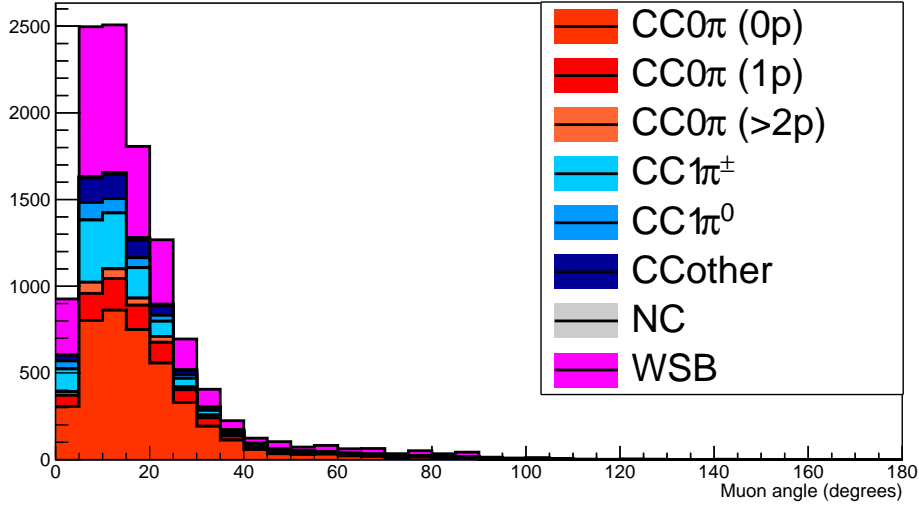


Figure 28: The reconstructed angles of the longest tracks in the selected events in the antineutrino-mode.

467 therefore help to constraint the particles that exits the WAGASCI module but do
 468 not geometrically enters any MRD.

- 469 • the particle identification of low momenta muons $p_\mu < 300$ MeV/c that will leave only
 470 few hits in the MRD. Using the WAGASCI module information will clearly enhance
 471 the particle identification.

472 This study is based on an original study done for the ND280 upgrade target, with some
 473 modifications. Though the cell size is similar to the WAGASCI configuration presented
 474 in Section 5, the external dimensions are different ($186.4 \times 60 \times 130$ cm 3). Whenever the
 475 results are presented with this external size and this parameter is likely to impact the
 476 result, it will be mentioned.

477 Note that in this section, a simplified reconstruction algorithm presented in Section 6.1 is
 478 used. The fiducial volume is chosen accordingly as the inner cube of the module which
 479 surfaces are distant of $4 \times$ scintillator space = 10 cm from the module external surfaces.
 480 The neutrino interactions are simulated using NEUT v5.3.2. The NEUT input neutrino
 481 flux is estimated using JnuBeam v13a and assuming the detector to be located at 1.5°
 482 off-axis, as in Section 5. Note that the event reconstruction efficiency as a function of true
 483 neutrino energy might be changed at 1.5° , due for example to different Q^2 distributions. For
 484 this reason, one has to note that the reconstruction results might slightly be changed from
 485 2.5° and 1.5° . To avoid a similar change on the particle-only reconstruction efficiencies,

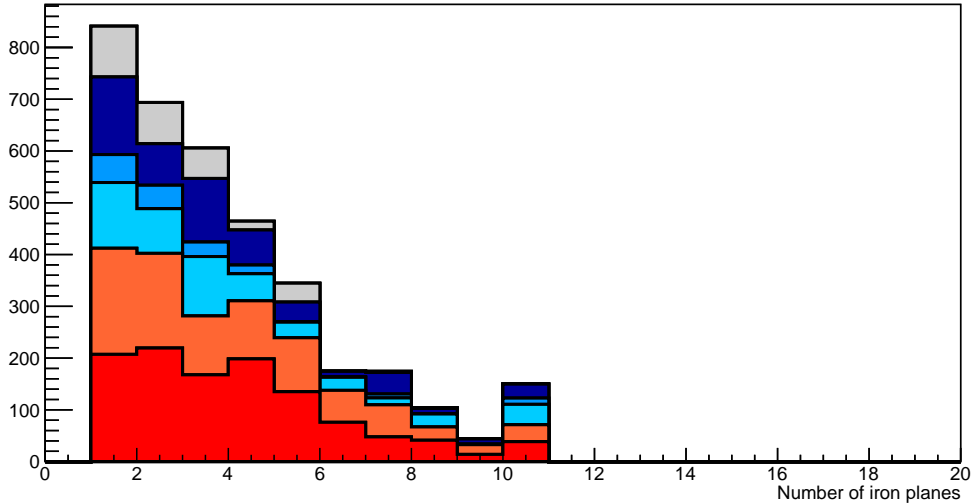


Figure 29: Iron plane numbers in Side-MRD corresponding to the end points of the longest tracks in the selected events in the neutrino-mode.

they will be presented as a function of variables that completely characterize the particle kinematic state, *i.e.* its momentum and angle. Figure 34 shows the vertices distributions of the daughter particles of neutrinos interacting one standard WAGASCI water-module. In this section, we will show the detector reconstruction and particle identification in this phase space, both for leptonic and hadronic particles. We will finally show an empty WAGASCI module can highly enhance the ability to constrain the neutrino interaction final state which is critical to reduce the corresponding uncertainties.

6.1 Reconstruction algorithm

6.1.1 Description

For this section, an ideal “simulated” reconstruction is developed. A particle is reconstructed if:

1. The particle is charged.
2. Lets at least one hit (energy deposit > 2.5 photo-electron) in a scintillator.
3. The particle enters one TPC and let one hit in the tracker.

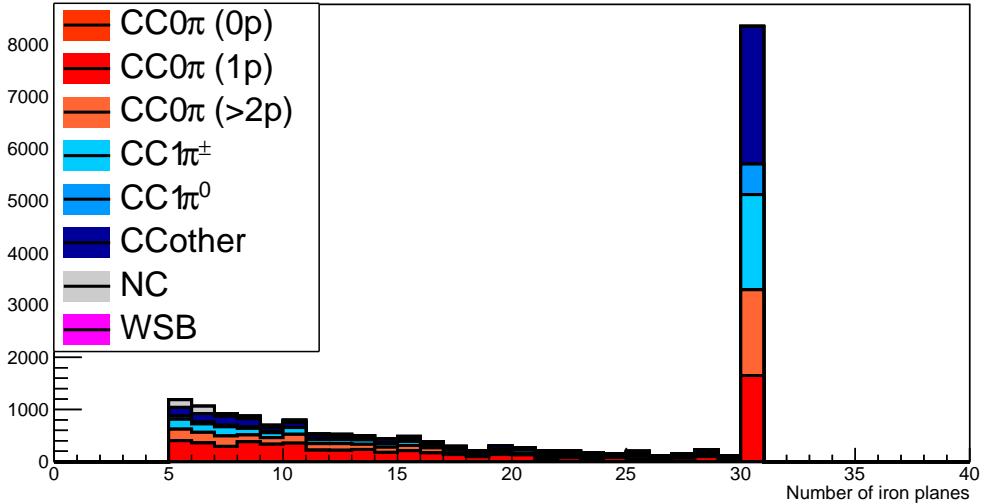


Figure 30: Iron plane numbers in Baby-MIND corresponding to the end points of the longest tracks in the selected events in the neutrino-mode.

501 Or

502

- 503 • The particle should be long enough to be reconstructed by the detector in at
504 least 2 out of 3 views (XZ, YZ, XY). The length criterion requires the particle
505 to let at least 4 hits in the detector. In the “less favourable case” of pure
506 longitudinal or transverse going tracks, it represents a the track length of $L_{track} \geq$
507 $4 \times$ scintillator space = 10.0 cm.
- 508 • In the views where particles pass the length criterion, the particle shall not
509 be superimposed with longer tracks in at least two views. The superposition
510 criterion is estimated with the distance inter-tracks (DIT) which corresponds to
511 the orthogonal distance between two tracks at the ending point of the shortest
512 one (see Figure 35). For a track 1, the superposition criterion is tested with
513 every longer tracks that starts at the same vertex. Let \vec{p}_1^i the vector of track
514 1, and p_1^q its projections in the XZ, YZ and XY planes respectively for $i=1,2,3$.
515 Note that these are projections in a 2D planes and not on a direction vector. In
516 this case, the relative angle between the track 1 and a longer track 2 (of vector

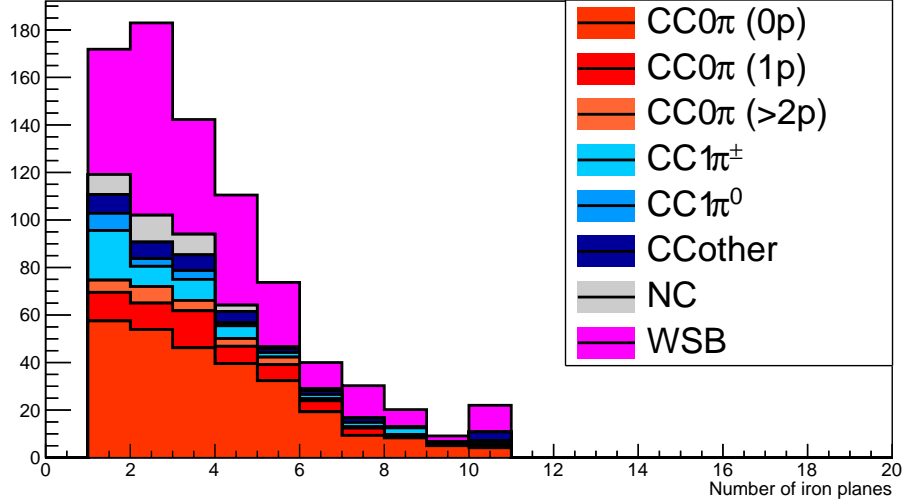


Figure 31: Iron plane numbers in Side-MRD corresponding to the end points of the longest tracks in the selected events in the antineutrino-mode.

517 \vec{p}_2) in a view a is given by:

$$\cos \theta = \frac{\vec{p}_1^a \cdot \vec{p}_2^a}{\|\vec{p}_1^a\| \|\vec{p}_2^a\|} \quad (1)$$

518 and the distance inter track is given by:

$$DIT = \|\vec{p}_1^a\| \sin \theta \quad (2)$$

519 The DIT should be higher than $4 \times$ scintillator width for the track 1 to be not
 520 superimposed with the track 2 in the view a, which also corresponds to 10.0 cm
 521 in the nominal configuration.

522 6.1.2 Performances

523 The particle-only reconstruction efficiencies and the reconstruction threshold in momenta
 524 are shown in Table 7. This threshold is defined as the maximal momentum for which the
 525 reconstruction efficiency is smaller than 30%. The thresholds in muon and pion momenta
 526 are 150 MeV/c. Most of the muons are above this threshold (see Figure 34) which leads
 527 to a 79% reconstruction efficiency.

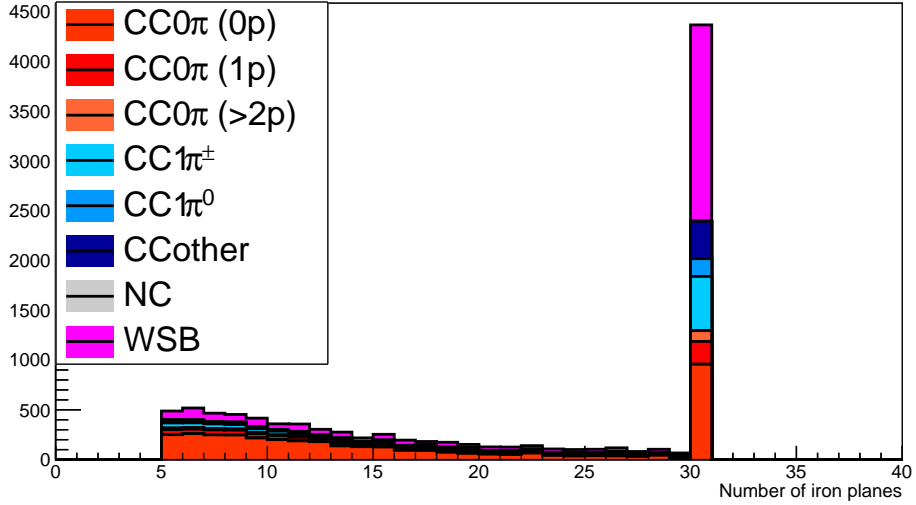


Figure 32: Iron plane numbers in Baby-MIND corresponding to the end points of the longest tracks in the selected events in the antineutrino-mode.

	μ	π	p
Reconstruction Efficiency	79%	52%	26%
Momentum threshold	150 MeV/c	150 MeV/c	550 MeV/c

Table 7: Reconstruction efficiency and momentum threshold for muons, pions and protons. The threshold is defined as the maximal momentum for which particles have a reconstruction efficiency smaller than 30%.

528 The lower pion and proton efficiencies (respectively 52% and 26%) are due to lower
 529 efficiencies for similar momenta than muons, coming from strong interactions as shown
 530 on Figures 36. Efficiencies of each particle type tend to decrease in the backward region
 531 due to particle lower momenta. However, for a fixed momentum value, the reconstruc-
 532 tion efficiency is almost uniform which confirms the ability of the WAGASCI detector to
 533 reconstruct high angle tracks.

534 The reconstruction is thereafter tested on neutrino events. Table 8 summarizes the
 535 number of reconstructed events and efficiencies for each interaction type. As expected
 536 from the high muon reconstruction efficiency, the charged current interactions have recon-
 537 struction efficiencies $\geq 85\%$.

538 The reconstruction efficiencies as a function of the neutrino energy and muon kinematics

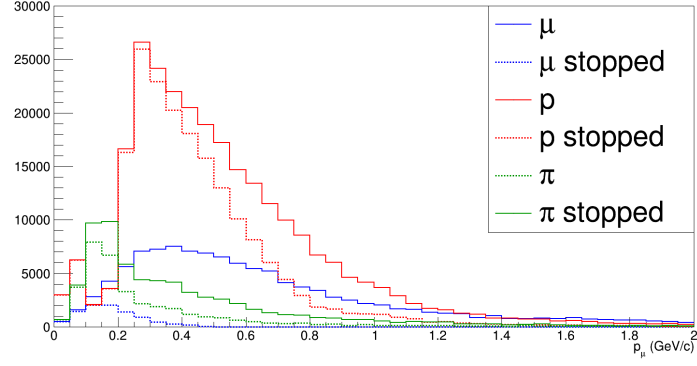


Figure 33: Momentum distribution of true particles in WAGASCI (plain) and corresponding distributions only for particles stopping into the WAGASCI module (dashed).

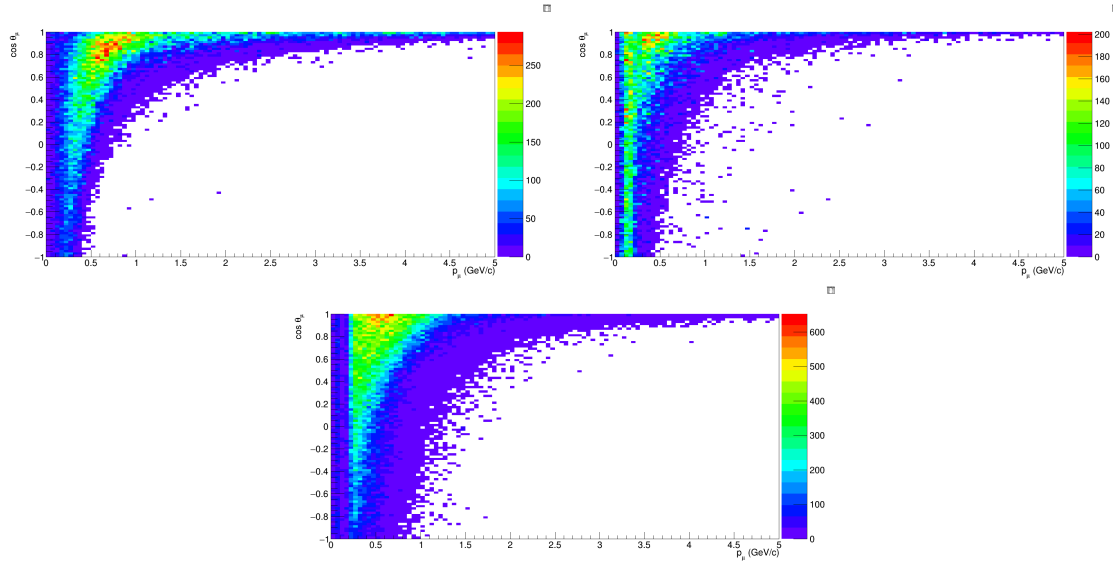


Figure 34: True number of muons (left), charged pions (right) and protons (bottom) in the two WAGASCI water-module as a function of the particles momenta and angles at 1.5° .

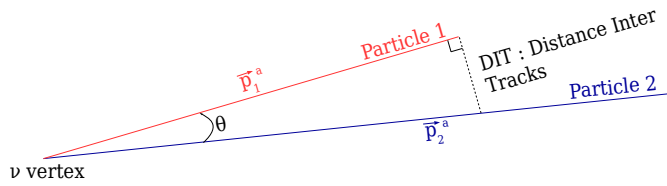


Figure 35: Definition of the distance inter tracks.

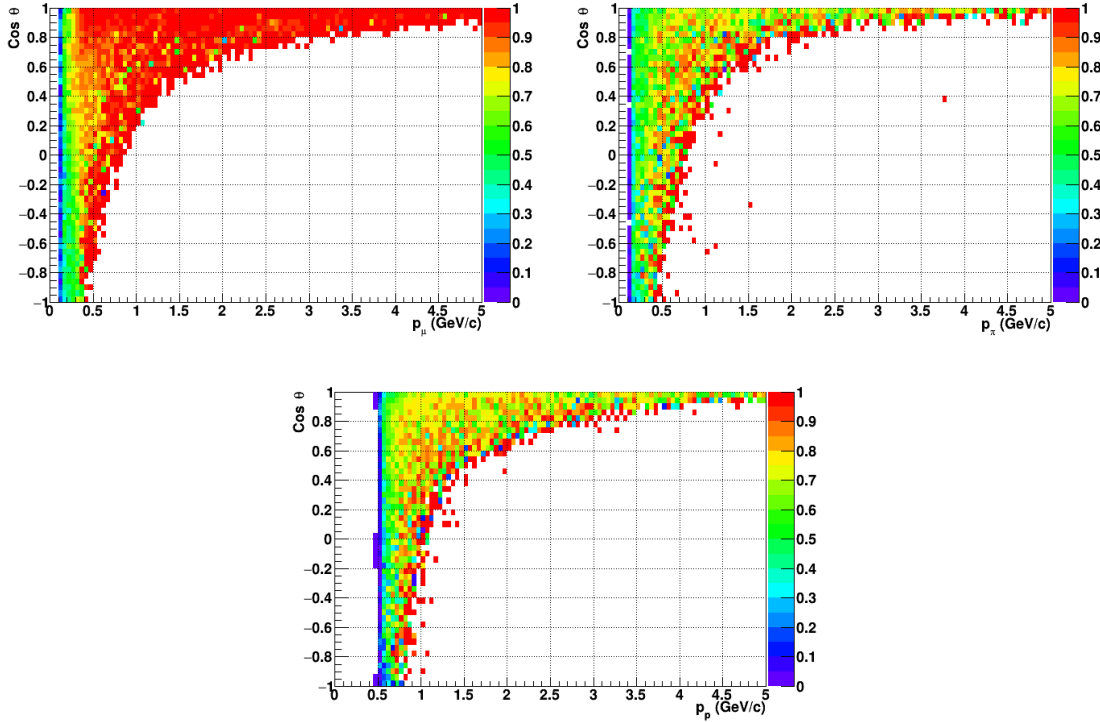


Figure 36: Reconstruction efficiency of muons (left), charged pions (right) and protons (bottom) in the WAGASCI water-module as a function of the particles momenta and angles.

	CC0 π	CC1 π	CCOthers	NC	All
Reconstruction efficiency	85%	87%	91%	22%	68%

Table 8: Number of true interactions reconstructed. The purity and reconstruction efficiency of each true interaction is also shown.

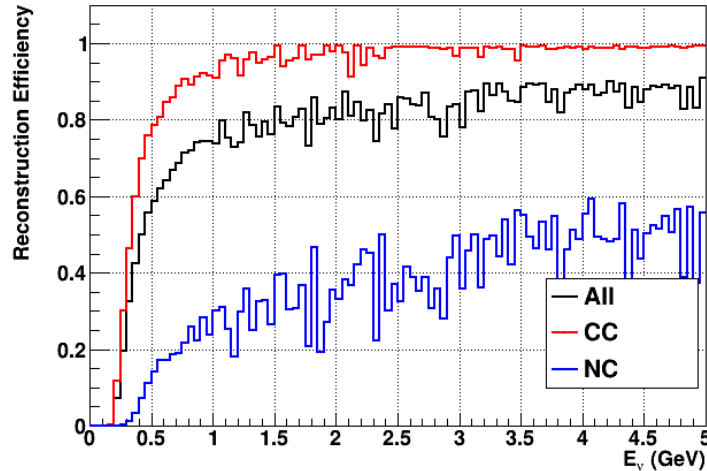


Figure 37: Reconstruction efficiency of all neutrino (black), CC (red) and NC (blue) interactions in the WAGASCI water-module as a function of the neutrino energy.

539 are respectively shown on Figure 37 and 38.

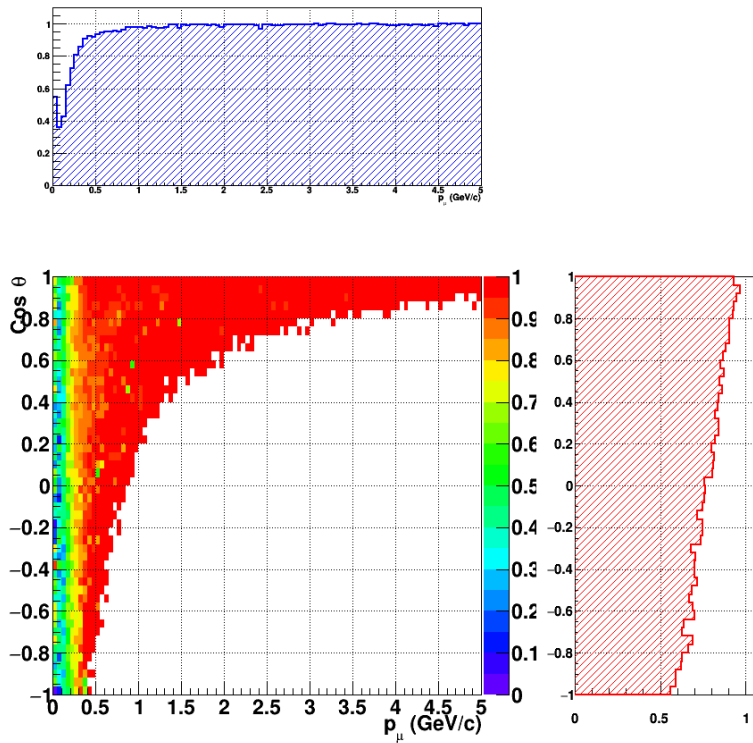


Figure 38: Reconstruction efficiency of CC interactions in the WAGASCI water-module as a function of the muon kinematic variables (momentum and angle).

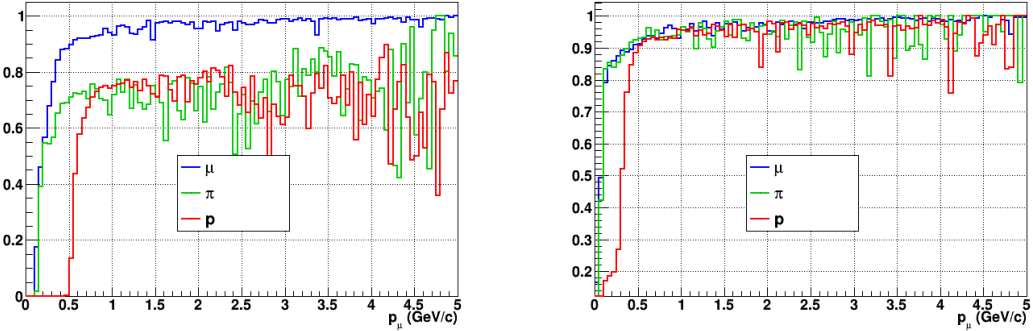


Figure 39: Reconstruction efficiency for muons, pions and protons in the water-in (left) and water-out (right) modules.

540 Note that a Particle Identification Algorithm has been also developed. It is based on
 541 the charge deposition of the particles in the scintillator, of the detection of a decay-electron.
 542 However, this information highly depends on the number of scintillator hit by a particle,
 543 which creates an important difference between a real WAGASCI module and the one used
 544 for the ND280-upgrade simulation. For this reason, the corresponding results will not be
 545 detailed here, but can be found in [?].

546 6.2 Background subtraction: the water-out module

547 In the nominal configuration, 20% of the neutrino interactions occurs on scintillators
 548 (C_8H_8). This background should be removed in order to measure the neutrino interac-
 549 tion on the same target as Super-K, which suppress the differences in cross-section models.
 550 For this purpose, we propose to use a water-out module, where the water is replaced by
 551 air. The detector is therefore fully active and has a 3 mm spatial resolution (scintillator
 552 thickness) which create an ideal detector to reconstruct and identify hadrons, and study
 553 np-nh interactions. The counter-part is the difference in particle energy deposition between
 554 the water and this water-out module that will need to be corrected for. In this section,
 555 we present the capabilities of such a module, and the impact it can have on cross-section
 556 measurements for the neutrino community in general and T2K in particular.
 557 The same reconstruction and selection as the water-in module is applied. Figure 39 shows
 558 the comparison between the water-in and the water-out reconstruction efficiencies for muon,
 559 pions and protons. 90% of the muons and 87% of the pions are reconstructed, while 70%
 560 of the protons are even reconstructed. It allows to lower down the proton threshold to
 561 250 MeV/c (see Table 9).

562 As a consequence of tracking even low momenta particle, the reconstruction efficiency
 563 is uniform and almost maximal on the entire $\cos \theta_\mu$ phase space, as shown on Figure 40.

	μ	π	p
Reconstruction Efficiency Momentum threshold	90% 50 MeV/c	87% 50 MeV/c	70% 250 MeV/c

Table 9: Reconstruction efficiency, proportions of μ -like and non μ -like and momentum threshold for muons, pions and protons in the empty module. The threshold is defined as the maximal momentum for which particles have a reconstruction efficiency smaller than 20%.

564 Since the fiducial mass represents 0.25 tons, the total number of events is divided by a
 565 factor of 3 compared to the water-in module. The water-out module offers interesting
 566 possibilities to study np-nh interaction since 70% of the protons are reconstructed. In the
 567 future, a possible separation as a function of the number of proton track will be studied.
 568 Moreover, we are currently pursuing the use of single and double transverse variables (cite
 569 Xianguo) to open new possibilities for separating np-nh from Final State Interactions, or
 570 for isolating the interactions on hydrogen from interactions on carbon in this module.

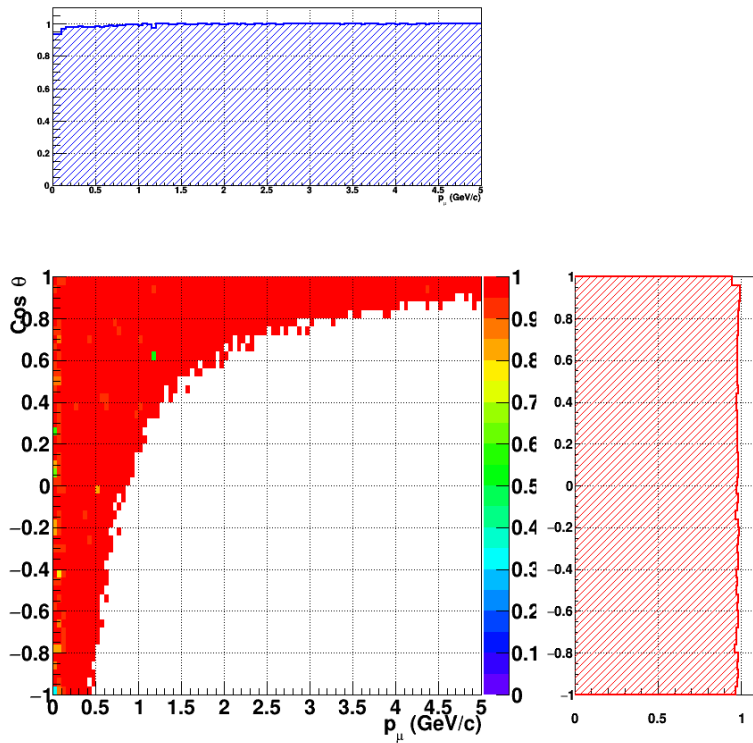


Figure 40: Reconstruction efficiency of CC interactions in the WAGASCI empty module as a function of the muon kinematic variables (momentum and angle).

571 **7 Schedule**

572 We would like to start a physics data taking from T2K beam time after the summer
573 shutdown in 2018. By then, commissioning and tests of the detectors will be completed
574 in J-PARC T59. The experiment can run parasitically with T2K, therefore we request no
575 dedicated beam time nor beam condition as discussed in the following section.

576 Once the approved POT is accumulated, the WAGASCI modules will be removed
577 from the experimental site, but we would like to keep the Baby-MIND and the Side-MRD
578 modules on the B2 floor of the NM pit as common platforms of future neutrino experiments
579 using the T2K neutrino beam.

580 **8 Requests**

581 **8.1 Neutrino beam**

582 The experiment can run parasitically with T2K, therefore we request no dedicated beam
583 time nor beam condition. As data taking periods, we request the ‘nominal’ T2K one-year
584 operation both for the neutrino beam and the antineutrino beam. The T2K has been
585 requesting 0.9×10^{21} POT/year and actually accumulating about 0.7×10^{21} POT/year in
586 recent years. For each year, starting from the Autumn, T2K is running predominantly in
587 the neutrino mode or in the antineutrino mode. Our request is to have one-year neutrino-
588 mode data and another one-year antineutrino mode data assuming that the POT for the
589 fast extraction in each year is more than 0.5×10^{21} POT.

590 **8.2 Equipment request including power line**

591 We request the followings in terms of equipment on the B2 floor:

- 592 • Site for the WAGASCI modules, Side-MRD modules and BabyMIND and their elec-
593 tronics system on the B2 floor of the near detector hall (Fig. 3).
- 594 • Anchor points (holes) on the B2 floor to secure the WAGASCI modules, Side-MRD
595 module and Baby-MIND (Fig. ??)
- 596 • Power line for the magnets in Baby-MIND: 400 V tri-phase 48-to-62 Hz, capable of
597 delivering 12 kW.
- 598 • Electricity for electronics and water circulation system, 3 kW, standard Japanese
599 electrical sockets.
 - 600 1. Online PCs: 2.1 kW
 - 601 2. Electronics: 0.7 kW
 - 602 3. Water sensors: ?

- 603 • Air conditioner for cooling heat generation at Baby-MIND magnets, online PCs and
604 electronics
- 605 • Beam timing signal and spill information
- 606 • Network connection

607 **8.2.1 Baby MIND Equipment request including power line**

608 We request the following in terms of equipment on the B2 floor:

- 609 • Site for the Baby MIND detector and its electronics systems on the B2 floor of the
610 near detector hall.
- 611 • Anchor points (holes) on the B2 floor to secure the 9 support frames, of order 4 holes
612 per frame, detailed floor plans to be communicated in a separate document.
- 613 • Power line for the magnet: 400 V tri-phase 48-to-62 Hz, capable of delivering 12
614 kW. We have a wish for the magnet power line to be installed and available to us by
615 beginning of March 2018.
- 616 • Electricity for electronics, 1 kW, standard Japanese electrical sockets.
- 617 • Beam timing signal and spill information
- 618 • Network connection

619 The infrastructure for much of the above exists already, and will be shared in part with
620 the WAGASCI experiment. Exceptions are the power line for the magnet and holes in the
621 B2 floor to anchor the detector support structures.

622 **9 Conclusion**